

Efficient, Fast, Low Power, Optical Phase Conjugation Using Two-Photon-Induced Zeeman Coherence in Rubidium

by

Emmanuel Rousseau

Ingénieur diplômé, Ecole Polytechnique (1993)

Ingénieur diplômé, Ecole Nationale Supérieure de Techniques Avancées (1995)

Submitted to the Department of Aeronautics and Astronautics
in partial fulfillment of the requirements for the degree of

Master of Science

at the

MASSACHUSETTS INSTITUTE OF TECHNOLOGY

February 1997

AERO

MASSACHUSETTS INSTITUTE OF TECHNOLOGY

FEB 10 1997

© Massachusetts Institute of Technology 1997
All rights reserved.

LIBRARIES

Signature of Author.....

Department of Aeronautics and Astronautics
December 18, 1996

Certified by.....

Shaoul Ezekiel
Professor of Aeronautics and Astronautics
and Electrical Engineering
Thesis Supervisor

Certified by.....

Dr. Selim M. Shahriar
Research Scientist, Research Laboratory of Electronics
Thesis Supervisor

Accepted by.....

Professor Jaime Peraire
Chair, Graduate Office

Contents

1	Introduction and Background:	5
1.1	A Brief Introduction to Optical Phase Conjugation:	6
1.1.1	Principle:	6
1.1.2	Mathematical Treatment:	9
1.1.3	Applications [1]:	10
1.2	Status of the Field:	18
1.2.1	General Considerations:	18
1.2.2	Raman OPC in Sodium [4]:	20
1.2.3	Perspectives of Raman OPC in Rubidium:	21
2	Zeeman Coherence Phase Conjugation:	23
2.1	Zeeman Hyperfine Levels:	24
2.2	Optical Pumping to a Lambda System:	26
2.3	Coherent Population Trapping:	27
2.4	Application to OPC:	32
2.4.1	Advantages of CPT:	32
2.4.2	Chosen Configuration:	33
3	Experimental Setup:	35
3.1	Main issues:	36
3.1.1	Optical System:	36
3.1.2	Atomic Vapor:	43
3.2	Design of the System:	45
3.2.1	Optics:	45
3.2.2	Vapor Cell:	46
4	Results:	50
4.1	Characterization:	51
4.1.1	Experimental Conditions:	51

4.1.2	CPT Diagnostic:	53
4.2	Additional Results:	60
5	Summary And Conclusions:	66
5.1	Summary and Conclusions:	67
5.2	Future work:	68

Abstract:

Optical phase conjugation (OPC) with low power and fast response is of interest in many applications. Generation of squeezed light, phase conjugation mirror, optical correlation and turbulence correction are the most promising examples.

Dye lasers and sodium atomic vapor have been used earlier within this group to demonstrate conjugation via hyperfine coherence gratings induced by coherent population trapping (CPT) in a Λ system. This resulted in a fast OPC (response time of about $1 \mu\text{s}$) with low pump intensities (about 1 W/cm^2). However this technique required that the probe be generated from the pump by coherent modulation at the hyperfine frequency difference of 1.77 GHz . In order to extend this technique to arbitrary atomic systems, one would require techniques for modulations at very high frequencies ranging from a few GHz (eg 6.8 GHz for rubidium, 9.2 GHz for cesium) up to hundreds of GHz (eg calcium and magnesium). As such, this technique is severely limited in practicality.

In order to circumvent this problem, we demonstrate in this thesis a new technique which uses the Zeeman sublevels within a hyperfine level as the two low-lying states of a Λ -transition. Specifically, we used the $5^2S_{1/2}, F = 2 \rightarrow 5^2P_{1/2}, F = 1$ transition of ^{87}Rb to demonstrate a reflectivity of 10 with a response time of 50 ns , using pump intensities of 2 W/cm^2 . Although we used a titanium:sapphire laser, these intensities are easily achievable using semi-conductor lasers, thus making it a very practical OPC system.

Acknowledgements:

I'd like first to thank Professor Shaoul Ezekiel, who gave me the opportunity to work on this research project.

Then I would like to thank Selim Shariar who always managed to find time for discussions and explanations, despite his busy schedule, his constant quest for lost sodas and coffee mugs.

Timothy Grove has been of great help when I had to learn all kind of practical skills in electronics, machining, vacuum techniques. . .

I would also like to thank all the people with whom I worked in the laboratory for the enjoyable atmosphere they created.

Finally, I'd like to apologize for my pioneer work on propulsion of photomultipliers by pressurised nitrogen, even if performances were quite impressive in the first but final attempt.

Chapter 1

Introduction and Background:

1.1 A Brief Introduction to Optical Phase Conjugation:

1.1.1 Principle:

Optical Phase Conjugation (OPC) via four-wave mixing is a third order non-linear effect involving four distinct waves interacting in an optical material¹.

Those four waves will be conventionally defined as:

- The *forward pump*, a ‘strong’ beam,
- The *backward pump*, another strong beam counterpropagating to the forward pump
- *The probe*, a ‘weak’ beam that is going to interact with the modification of the OPC material induced by the two pumps,
- *The conjugate* beam, that will be defined as the result of the total interaction, its denomination being justified later.

The physical principle of the interaction can be seen as a diffraction of light from gratings induced in the OPC material by the interference of the existing beams. The details of the process creating the grating doesn’t need to be inspected for the comprehension of OPC, but will, of course, be essential when efficiency, response time, or any other practical issue will be examined.

For the sake of argument, we assume that the amplitude of the grating at a given point of the material is simply proportional to the local intensity of the total electric field of the interfering beams there. The problem is then purely geometrical, defined by the positions and directions of propagation of the beams.

We consider two plane waves interfering, the two electric fields can be written as:

$$\vec{E}_i = \vec{E}_i^0 e^{j(\omega_i t - \vec{k}_i \cdot \vec{r})} \quad (i \in \{1, 2\})$$

The local intensity is then:

$$I = |\vec{E}_1^0 + \vec{E}_2^0|^2$$

The only important result of the development of this expression is that the local intensity is modulated as:

$$\cos[(\omega_1 - \omega_2)t - (\vec{k}_1 - \vec{k}_2) \cdot \vec{r}]$$

So if we consider the diffraction of a third plane wave from the moving grating, the phase of any field generated is given by:

¹Examples include photo-refractive crystals, atomic vapors, optical fibers etc...

$$(\omega_1 - \omega_2 + \omega_3)t - (\vec{k}_1 - \vec{k}_2 + \vec{k}_3) \cdot \vec{r}$$

If we focus our attention on a particular plane wave, generated by the previous process, its phase is given by:

$$\omega_4 t - \vec{k}_4 \cdot \vec{r}$$

For this scattered wave to build up it is necessary that the diffraction pattern and this wave are in phase at any point and at any time. This condition is called *phase matching* and is an essential concept of Non-Linear Optics. To respect phase matching, the two following conditions have to be met:

$$\omega_1 + \omega_3 = \omega_2 + \omega_4 \quad (1.1)$$

$$\vec{k}_1 + \vec{k}_3 = \vec{k}_2 + \vec{k}_4 \quad (1.2)$$

Under certain conditions, these two relations can be viewed as a consequence of conservation law in quantum mechanics:

- Using Planck's Law ($E = h\nu$), equation 1.1 can be seen as a conservation of energy relationship,
- Using De Broglie's Law ($\vec{p} = \hbar\vec{k}$), equation 1.2 can be seen as a conservation of momentum relationship.

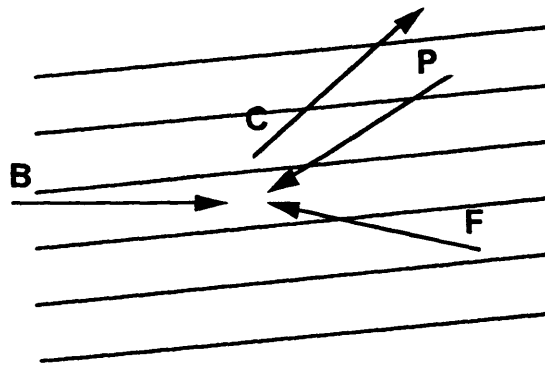
Following this idea, the global process can be reinterpreted using the photon concept: two photons are annihilated (1 and 3), while two new photons are created (2 and 4). This is consistent with a third order Non-Linear process.

Now coming back to our particular case, using again the diffraction picture, it is natural to label the pumps as the energy depleted waves, whereas the probe and the conjugate are labeled as the amplified waves. Two particular processes explain the generation of the conjugate (cf figure 1.1):

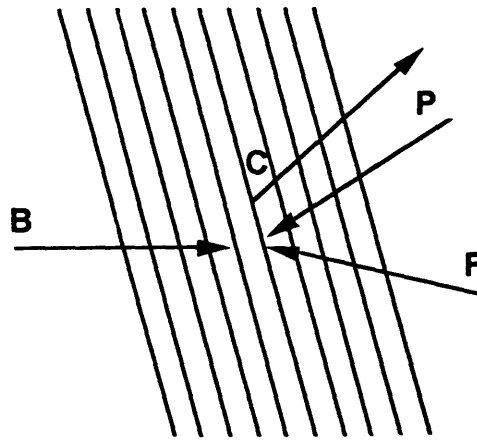
- Generation of a new beam, the conjugate, by diffraction of the forward beam from the moving grating generated by interference of the probe and backward beam,
- Some more generation of the conjugate, by diffraction of the backward beam from the moving grating generated by interference of the probe and forward beam.

Similarly, we can explain the simultaneous amplification of the probe by the two following processes:

- Amplification of the probe, by diffraction of the backward beam by the moving grating generated by interference of the conjugate and forward beam,



Scattering of the backward beam from the grating created by the interference of the probe and forward beams



Scattering of the forward beam from the grating created by the interference of the probe and backward beams

Figure 1.1: Moving gratings involved in generation of the conjugate

- Amplification of the probe, by diffraction of the forward beam by the moving grating generated by interference of the conjugate and backward beam.

One essential issue is that the spatial period of the two gratings are different, the grating corresponding to the interference of the probe and backward beams has a small spatial period, so that this grating can be easily washed out by any perturbation in the medium. Consequently the other grating is a priori a more efficient source of OPC.

It is important to note here that the generation of the conjugate is not made by depleting the probe, but that the energy is taken from the pump beams.

The most interesting feature of OPC is contained in the phase relationship between the probe and the conjugate, which are out of phase with respect to each other². This explains the denomination of the conjugate, its complex amplitude being proportional to the conjugate of the complex amplitude of the probe.

Another valuable feature is that spatial phase-matching is automatically respected. Whatever the respective orientations of the beams are, the probe is always going to be amplified and the conjugate is always going to come out of the OPC material.

1.1.2 Mathematical Treatment:

To get some more quantitative results, we consider here the simple case of four wave mixing:

- The material is isotropic,
- All the beams are plane waves at the same frequency,
- We neglect absorption,
- The two pumps are strictly counterpropagating, along the z axis,
- The probe is weak and we can neglect depletion of the pumps.

Under such conditions, the third order behavior of the OPC material is given by $\chi_{xxxx}^{(3)}(\omega, -\omega, \omega)$, and the evolution of the complex amplitudes is given (in

²This will be shown explicitly in the mathematical treatment of OPC.

cgs units) by:

$$\begin{aligned}\frac{\partial A_C}{\partial z} &= j \frac{4\pi^2}{n\lambda} \chi^{(3)} A_F A_B A_P^* \\ \frac{\partial A_P}{\partial z} &= -j \frac{4\pi^2}{n\lambda} \chi^{(3)} A_F A_B A_C^*,\end{aligned}$$

where A_F, A_B, A_P, A_C are the complex amplitudes of, respectively, the forward, backward, probe and conjugate beams, n is the index of the medium and λ is the wavelength.

We use the notation:

$$\alpha = j \frac{4\pi^2}{n\lambda} \chi^{(3)} A_F A_B$$

The two equations are easily solved considering that the pumps are constant, and using the boundary conditions, for an interaction length L :

- $A_C(L) = 0$
- $A_P(0)$ given.

The amplitudes are found to be:

$$\begin{aligned}A_P(z) &= \frac{A_P(0)}{\cos|\alpha|L} \cos(|\alpha|(L-z)) \\ A_C(z) &= -\frac{\alpha A_P^*(0)}{|\alpha| \cos|\alpha|L} \sin(|\alpha|(L-z))\end{aligned}$$

The resulting intensities are:

$$\begin{aligned}I_P(L) &= \frac{I_P(0)}{\cos^2|\alpha|L} \\ I_C(0) &= I_P(0) \tan^2|\alpha|L\end{aligned}$$

This shows that the probe is always amplified and that the conjugate signal can rapidly be stronger than the probe if $|\alpha|L$ is big enough. One can see that $I_P(L) - I_C(0)$ is constant, which is consistent with the quantized view.

1.1.3 Applications [1]:

We shall begin with a kind of generic device that can be designed using OPC, that is the Phase Conjugation Mirror (PCM). For the sake of argument, let's

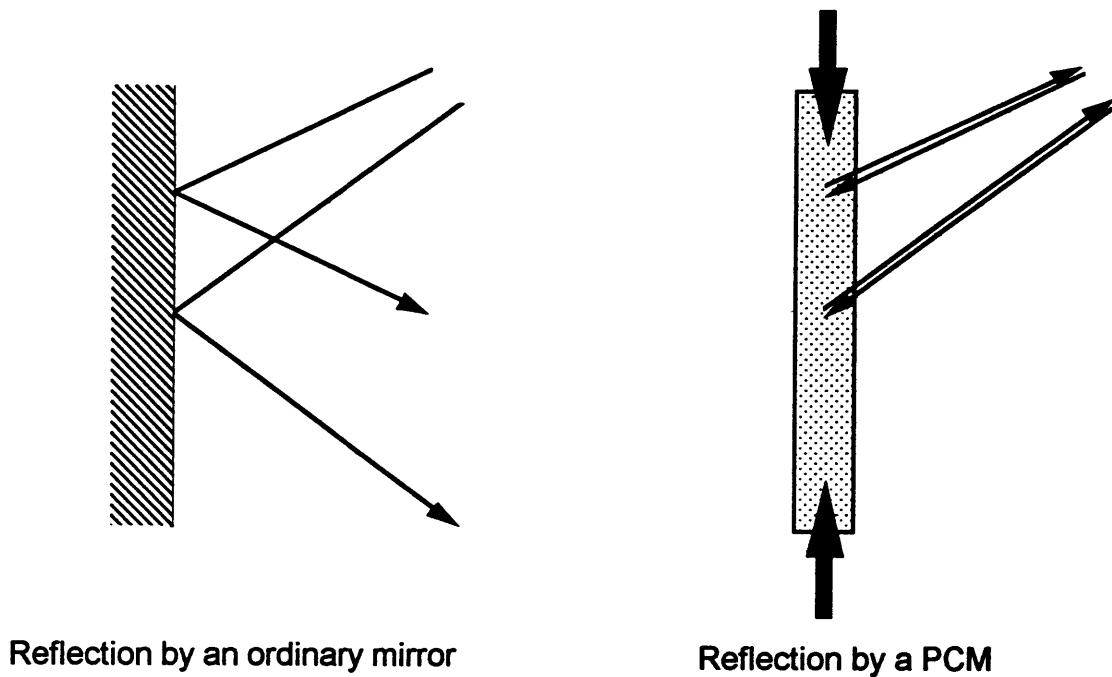


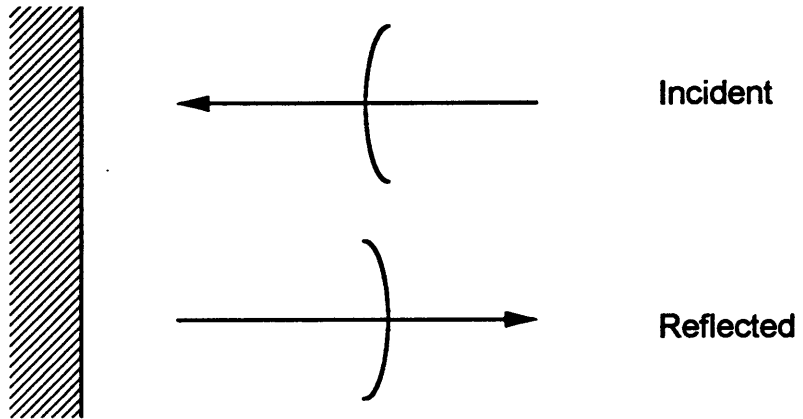
Figure 1.2: Comparison of a PCM and an ordinary mirror

consider the simplest case: the two pumps have the same frequency and are perfectly counterpropagating. These conditions met, the conjugate beam has the same frequency as the probe and is perfectly counterpropagating with respect to the probe. This last property makes the PCM totally different from an ordinary mirror, which simply reflects the incoming light: a PCM ‘reflects’ it back in the direction of incoming light (cf figure 1.2).

To understand the major interest in OPC, one needs to consider the wavefront after reflection from a PCM. An ordinary mirror will flip the incoming wavefront, but a PCM is going to send it back unmodified (actually as if light traveled back through time) as shown in figure 1.3.

This is extremely useful, because this property can be used to correct distortion due to propagation through a distorting material. For a plane wave traveling through a material with a higher index core, its wavefront is going to be delayed where the index is high. If we place an ordinary mirror in its path to reflect it back, the wavefront is going to be delayed the same way it was before, doubling the aberration. If we replace this mirror by a

(a)



(b)

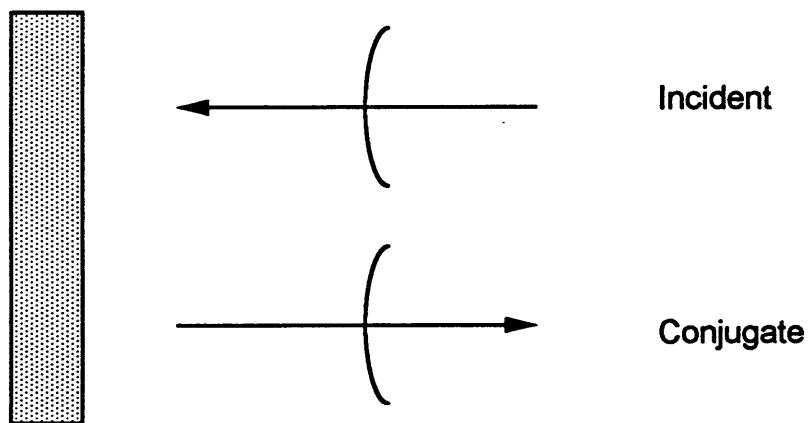


Figure 1.3: Reflection of a wavefront from an ordinary mirror and from a PCM

PCM, the wavefront is not going to be flipped. Rather it is going to travel back with the same wavefront, and seeing the same delay, the wavefront will be regenerated as it was before (cf figure 1.4).

This was only a simple case, but as far as the aberrating material is linear the correction will work. Furthermore, since phase-matching is virtually insensitive to geometry, this correction can be made with any pattern: even small details corresponding to high spatial frequency will be restored. Application of this are numerous, but one is particularly interesting. A PCM can be used to correct the distortion due to atmospheric propagation, without any kind of signal processing and in an instantaneous way (cf figure 1.5). This can be used to provide a laser communication channel to a plane or a satellite that is virtually insensitive to all kind of turbulences that would plague a simple laser system. For instance, the plane can send a laser beam to a receptor constituted by a PCM. Modulation of its reflectivity can be used to code a signal that will not be affected by propagation when it travels back to the plane. This is of course only possible due to the speed of light: the round-trip time is so short that the turbulences don't have time to change enough to disable the system.

Another good example of application of a PCM is its use in Laser technology. Indeed, in a linear configuration you can replace the mirror opposite to the output coupler with a PCM (cf figure 1.6). The advantages are obvious:

- The laser is virtually non sensitive to misalignement,
- The laser beam has an extremely good spatial quality, thanks to the correction of distortion.

This idea has actually been implemented, the quality of the beam being good enough to overcome the problem of power used by the PCM.

A more simple use of a PCM is targeting on a fusion material. The idea is simply to illuminate the target with a low power laser. This light scatters and eventually one part reaches the PCM, which in return can send back a much more powerful light (the amplified conjugate) right on the target (cf figure 1.7).

Another application results from a simple fact: OPC is equivalent to real time holography. In holography, the image is read by scattering a strong laser beam on the grating engraved in the material by the interference of a counterpropagating beam and the object beam (cf figure 1.8). Similarly we can consider the generation of the conjugate as a reading, by the backward beam, of the hologram instantaneously written by the interference of the

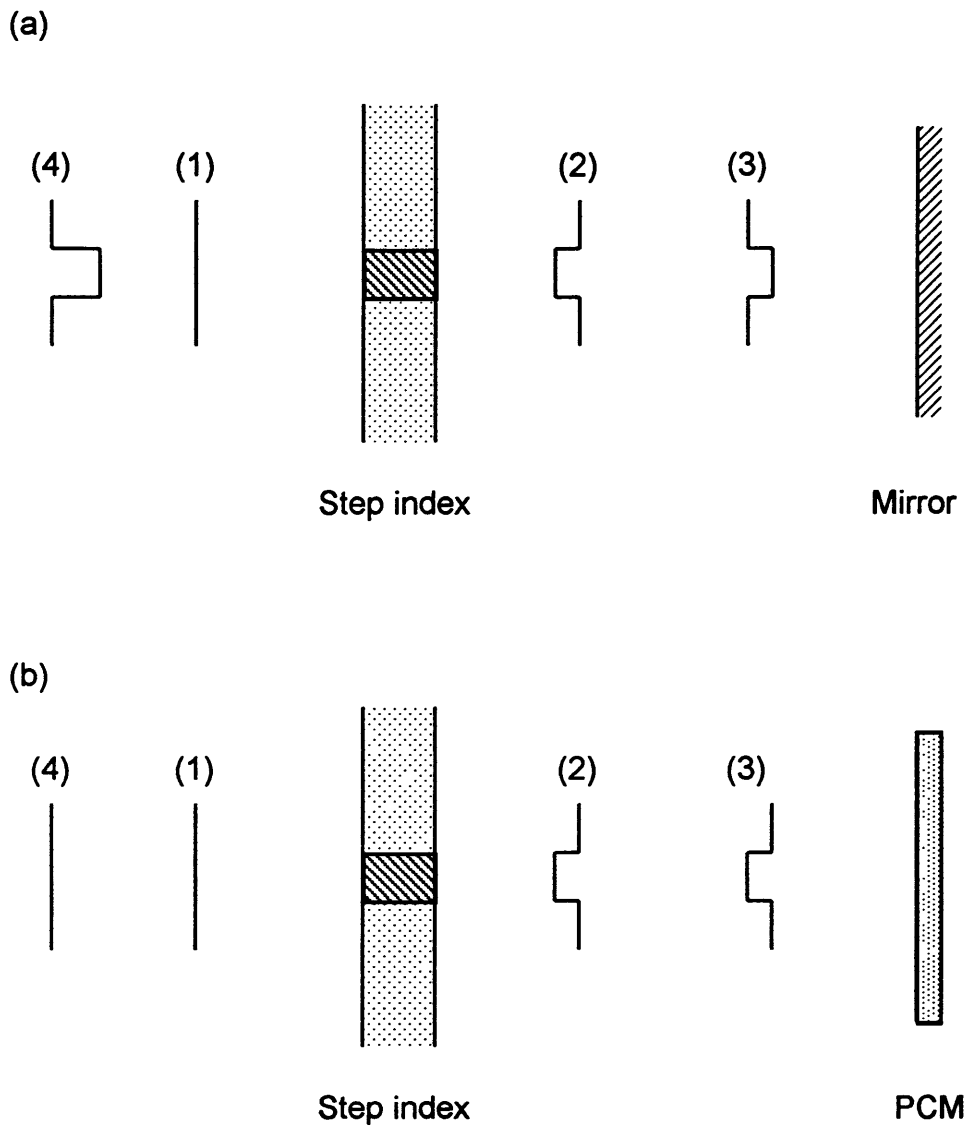


Figure 1.4: Correction of distortion of light using a PCM

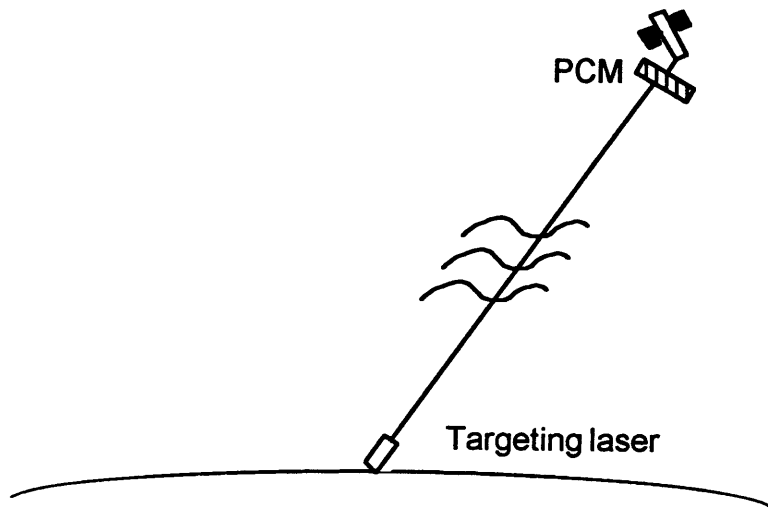


Figure 1.5: Correction of atmospheric propagation

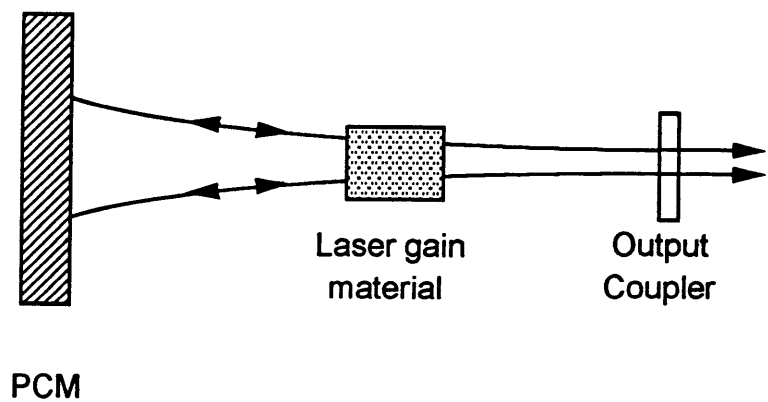


Figure 1.6: Laser setup using a PCM

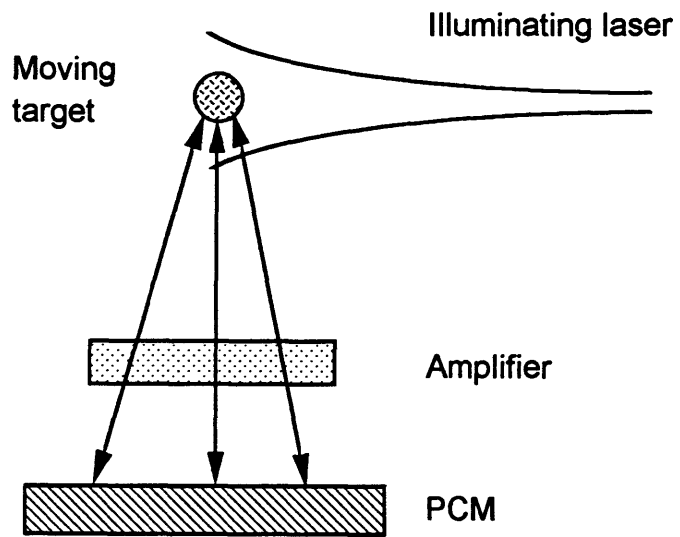


Figure 1.7: Targeting device using a PCM

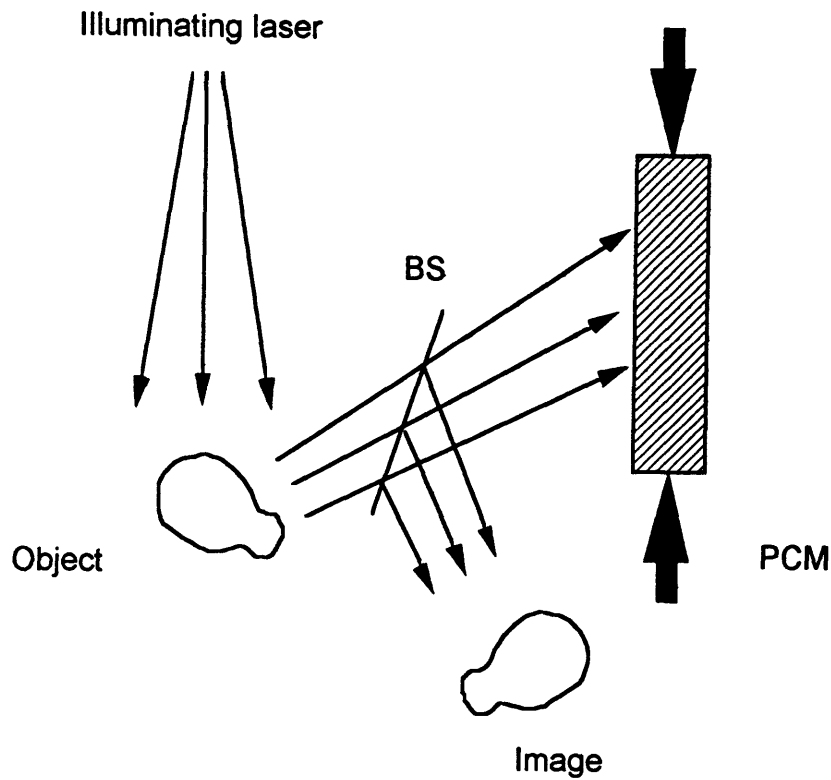


Figure 1.8: Real time holography by OPC

probe and the forward beam. Thus OPC can be used as a way of generating real time holograms, which can be used in applications like real time data storage and retrieval among others.

We mention the fact that OPC can be used to generate a special kind of light, squeezed light, which corresponds in practice to a reduction of the noise on the intensity below the shot-noise limit [2]. This can be used to design enhanced interferometers that have a greater sensitivity than the usual setup, and thus OPC can be very useful in high precision measurements.

Finally, OPC can be applied to optical correlation. The process is based upon the fact that the conjugate signal is (in the linear regime, that is for low probe power) proportional to the product of the complex amplitude of the pumps and to the complex amplitude of the probe. Using a lens you can generate a bi-dimensional Fourier transform of one pump and the probe,

which creates a conjugate (in the low probe power regime) given by:

$$A_c \propto F[E_F]F[E_P]^*$$

The conjugate then travels back through the lens which creates the inverse Fourier transform:

$$F^{-1}[F[E_F]F[E_P]^*] = \int E_F(x + x', y + y')E_P^*(x + x', y + y')dx'dy'$$

This means that the conjugate signal is proportional to the cross-correlation function of the two images. Such a design has been realized by Biaggio et al. in an atomic vapor of caesium [3]. Figure 1.9 presents the setup and some results. Thus OPC is a real good candidate for massive parallel two-dimensional signal processing.

1.2 Status of the Field:

1.2.1 General Considerations:

Since OPC has many promising applications, it is of major interest to investigate devices that could achieve it as easily as possible. The final goal is to find a material and a process that could be implemented as an electro-optic component, without overwhelming technical difficulties and with as great advantages as possible. In fact material factors explain the paucity of applications that are made of OPC, it is simply difficult to get an OPC material having a reasonable combination of properties.

To make OPC practical, we focus our attention on three particular material properties: response time, power threshold and gain (reflectivity). The response time is essentially the time required to write the gratings. If the OPC material moves during the writing process, the grating is going to be distorted and this will affect the quality of the conjugate (the phase matching is going to be approximate). This means that the response time must be short compared with a typical time scale of the motion of the medium. In a crystal this time corresponds to the period of acoustic vibrations, while in a vapor it is the average time required by an atom to cross the most effective grating. To get in the range of practical applications, $1 \mu s$ is a reasonable estimate of the time response required.

The power threshold is the minimal power we need to make the OPC process work. This threshold has to be as low as possible, this issue being of course more sensitive for signal processing applications than for fusion applications, where the big laser is already necessary. An intensity of $1 W/cm^2$ for a 1 mm spot size seems a reasonable requirement for applications. This corresponds to a $10 mW$ power that can be easily achieved with low cost lasers (semi-conductor lasers for instance).

(a)

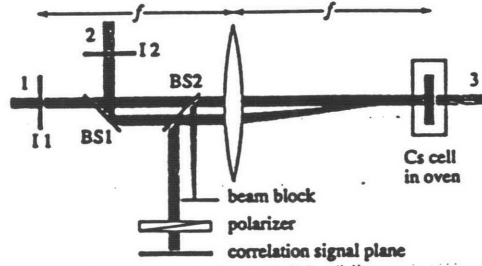


FIG. 1 Schematic of the optical correlator. Laser beams 1 and 2 pass through the image masks I1 and I2. The beams are then made parallel to each other by beam-splitter BS1 and are focused by the lens (with a focal length $f=127$ mm). The Fourier transforms of the images overlap in the cell containing the caesium atoms. Laser beam 3, collimated to a diameter of 5 mm, interacts with the other two beams in the caesium-containing cell and produces the signal beam, which is Fourier-transformed by the lens, reflected by beam splitter BS2, and detected by the CCD array of a video camera. Beams 1 and 2 are polarized perpendicular to the plane of the figure. Beam 3 and the signal beam are polarized in the plane of the figure. The polarizer in the path of the signal beam suppresses undesired scattered light from beams 1 and 2.

(b)

FIG. 2 Cross-correlation table of images of the three letters A, B, C. The columns and the rows in the plot are labelled with A, B and C. The correlation function of image 1 and image 2 is found in the first row and second column, and in the second row and first column. The peaks on the diagonal correspond to equal images being input into the correlator. a, Mathematical calculation of the expected intensity pattern at the output of the correlator. The square $|E_c(x,y)|^2$ of the amplitude correlation function is plotted as a function of the x,y coordinates. b, Combined results of nine experiments. The letters on the masks are $230 \mu\text{m}$ tall. The input power on beam 1 is $80 \mu\text{W}$ and the input power on beam 2 is $420 \mu\text{W}$. Beam 3 passes through a 3-mm aperture and has a power of $40 \mu\text{W}$. The intensity corresponding to the peak of the autocorrelation of C is $0.27 \mu\text{W cm}^{-2}$. The powers of the two image-bearing beams given here are the ones that can be measured just before beam splitter BS2 (see Fig. 1). The intensity of the signal beam is the one just after beam splitter BS2.

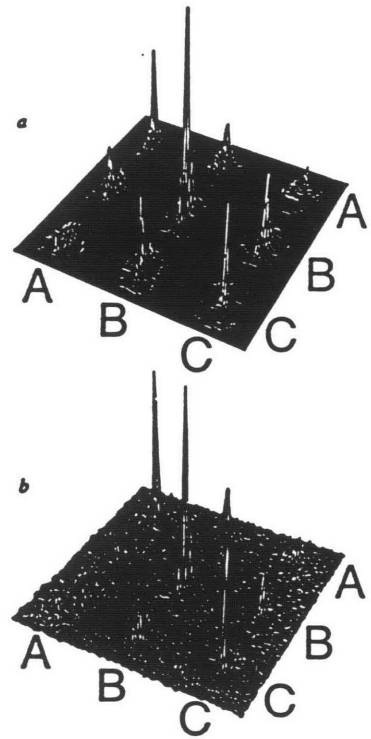


Figure 1.9: (a) OPC correlation setup (b) Results

Material	τ_r	I_{th}	R
Brillouin scattering	1-10 ns	1-10 MW/cm ²	≈ 1
Quantum Well	1 ps-1 μs	1 W/cm ²	≈ 0.03
Two level Na	10-100 ns	100 W/cm ²	2-3
Photorefractive (BaTiO ₃)	10 ms	≤ 1 W/cm ²	≥ 10
Double Λ Na	≤ 1 μs	1 W/cm ²	≥ 50

Table 1.1: Material properties of various OPC media

Finally, it is interesting to get a reflectivity better than one. This issue can be justified by the signal to noise ratio issue, where it is always better to amplify before trying to do any processing. If OPC is to do both the amplification and the treatment at the same time, it is necessary to have a reflectivity above one is a reasonable goal. Also high reflectivity is important for squeezing applications.

Given that there is a variety of possible mechanisms responsible of the formation of gratings, it comes as no surprise that many media can be used for OPC. The simplest case is the usual volume hologram. OPC has been made using a variety of nonlinear optical effects such as Brillouin scattering, photorefractive crystals, two level alkali atoms and quantum wells (pulsed regime). But none of these methods satisfy all the criteria simultaneously. Usual holography has a very long time response, ie the development time of the plate. Brillouin scattering requires very high intensities (1 MW/cm²). Quantum wells are inherently fast (picosecond regime), but have very low reflectivity and don't work at room temperature. Two level resonant alkali vapors are fast (nanosecond regime) and can exhibit high gain, but still require too much power (100 W/cm²). These parameters are summarized in table 1.1.

1.2.2 Raman OPC in Sodium [4]:

Raman OPC using a double Λ resonant configuration in sodium has been shown to have promising performances (cf table 1.1). Unfortunately the characteristics of the process lead to some practical difficulties.

The transitions used are in the D_1 transition of sodium, which is in the visible range (around 589 nm). Such a wavelength already eliminates the possibility of using basic semi-conductor lasers, that are currently limited to the infra-red part of the spectrum ($\lambda \geq 650nm$). This explains the use of two ring dye lasers to generate the two pumps, which is quite impractical. But a more important problem is the fact that this technique requires modulation

of one pump to a frequency equal to the hyperfine ground states separation. In sodium this is only 1.77 GHz, but for other materials, like calcium or magnesium, it can reach a few hundreds of GHz.

What is needed is a scheme which uses the Raman process to yield low-power and efficient OPC, but uses nearly degenerate frequencies. In this thesis, we present such a scheme using the Zeeman hyperfine sublevels of ^{87}Rb for writing gratings. Although we demonstrate this scheme with rubidium, the scheme is so generic that any atomic or molecular system can be used.

The most interesting result of this experiment was the interpretation of the OPC process. Coherent Population Trapping (CPT) has been identified as source of OPC, and seems quite promising. This has led to the idea of the presented experiment that was designed to use CPT in a vapor of rubidium, circumventing the problem of modulation. CPT will be analyzed in the next chapter.

1.2.3 Perspectives of Raman OPC in Rubidium:

Rubidium is an alkali, so that its properties are similar to those of sodium. But an interesting difference is that the D_1 line corresponds to infra-red (795 nm), which can be obtained with semi-conductor lasers.

Unfortunately, use of the same double lambda configuration as in sodium is difficult because the separation of the two corresponding ground states is 6.8 GHz. Such a shift cannot be achieved with an AOM, it requires the use of an electro-optic modulator or direct modulation of the diode laser current. A problem then arises from the colinearity of the shifted and unshifted beams. The unwanted frequencies have to be filtered out, which is not simple at all. Furthermore, such a modulation would be simply impossible for applications that would require atoms that have a much larger ground states splitting, like for example calcium or magnesium, that have splitting of a few hundreds of GHz.

This problem can be circumvented by using CPT within a different system consisting of the Zeeman sublevels within an hyperfine sublevel. Since hyperfine levels are well separated in rubidium, the process can be easily analyzed and interpreted.

The first advantage is that the pump and forward beams have to be detuned by only approximately 60-80 MHz, which can be achieved with an AOM with only one laser, or with two lasers slightly detuned.

The most important advantage is that the probe beam doesn't need to be detuned from the forward beam when there is no magnetic field, which

simplifies the system. However, to be able to make some diagnosis, like using a given magnetic field, a small detuning has been made possible in the experimental setup.

Chapter 2

Zeeman Coherence Phase Conjugation:

2.1 Zeeman Hyperfine Levels:

The initial calculations of atomic levels can be made without taking into account the nuclear spin, which reduces the expression of the total angular momentum to:

$$\vec{J} = \vec{L} + \vec{S},$$

where \vec{L} is the orbital angular momentum and \vec{S} is the electron spin. The experiment we made uses a more subtle feature involving the hyperfine levels, so we need to use a more accurate description that includes the spin of the nucleus \vec{I} . The total angular momentum is then:

$$\vec{F} = \vec{L} + \vec{S} + \vec{I},$$

One description of the state of the atom can then be made by using the following quantum numbers: L, S, J, I, F and m_F , where:

- L is the magnitude of the orbital angular momentum,
- S is the magnitude of the electron spin,
- J is the magnitude of $\vec{L} + \vec{S}$,
- I is the magnitude of the spin of the nucleus,
- F is the magnitude of the total angular momentum,
- m_F is the value of the projection of \vec{F} on the quantization axis.

Now we must consider the electric dipole observable, to be able to calculate the matrix elements of the interaction:

$\vec{\mu} = -e\vec{r}$, where e is the absolute value of the charge of the electron and \vec{r} is the position of the electron, with respect to the center of mass of the nucleus. To use the tensorial operators formalism, we use the following coordinate system:

$$\begin{aligned}\hat{-1} &= \frac{1}{\sqrt{2}}(\hat{x} - i\hat{y}) \\ \hat{0} &= \hat{z} \\ \hat{1} &= -\frac{1}{\sqrt{2}}(\hat{x} + i\hat{y})\end{aligned}$$

The components of $\vec{\mu}$ in this coordinate system are written as $\mu_q (q \in \{-1, 0, 1\})$. We can then use the Wigner-Eckart theorem to derive that:

$$\begin{aligned}\mu_q &= \langle \gamma' L' S' J' I' F' m_{F'} | \mu_q | \gamma LSJIF m_F \rangle \\ &= \frac{1}{\sqrt{2F'+1}} \langle F1m_{F'} q | F1F' m_{F'} \rangle \langle \gamma' L' S' J' I' F' || \mu_q || \gamma LSJIF \rangle,\end{aligned}$$

where $\langle \gamma' L' S' J' I' F' || \mu_q || \gamma LSJIF \rangle$ is the reduced matrix element and $\langle F1m_{F'} q | F1F' m_{F'} \rangle$ is a simple Clebsch-Gordan coefficient and γ represents all the other quantum numbers. The Clebsch-Gordan coefficient yields the following selection rules:

$$\Delta F = \pm 1, 0 \quad (2.1)$$

$$F + F' \geq 1 \quad (2.2)$$

$$\Delta m_F = q \quad (2.3)$$

This is extremely important since it allows us to know what are the possibly permitted transitions and to know which polarization of light can couple two levels:

- Linearly polarized light along \hat{x} is going to couple states with the same component of F ,
- Circularly polarized light σ_{\pm} is going to couple states for which $\Delta m_F = \pm 1$.

Once these hyperfines sublevel are defined, we can calculate the Zeeman shift produced by a magnetic field along the quantization axis. The perturbation Hamiltonian is:

$$H_{ext} = g_J \mu_B \vec{B} \cdot \vec{J} - g_I \mu_B \frac{m_e}{m_N} \vec{B} \cdot \vec{I},$$

where g_J, g_I are the Landé g-factors, μ_B is the Bohr magneton, m_e is the mass of the electron, and m_N is the mass of the nucleus.

It is then possible to express the Zeeman shift as:

$$\Delta E = g_F \mu_B,$$

where the g-factor is now:

$$g_F = \left[\frac{3J(J+1) + S(S+1) - L(L+1)}{2J(J+1)} \right] \left[\frac{F(F+1) + J(J+1) - I(I+1)}{2F(F+1)} \right].$$

Here we used the fact that the mass of the electron is much smaller than the mass of the nucleus to neglect a second contribution.

2.2 Optical Pumping to a Lambda System:

Interaction of Zeeman sublevels and polarized light obeys selection rules that can be used to obtain special population distribution by what is called *Optical Pumping*. The basic picture can be obtained by considering a $F = 1 \rightarrow F' = 1$ transition. First, those values of F and F' respect the selection rules 2.1 and 2.2, so that the transition is a priori possible. But considering 2.3, we can see that only a few transitions can be induced by interaction with circularly polarized light:

Furthermore, additional selection rules (which follow, for example, from an

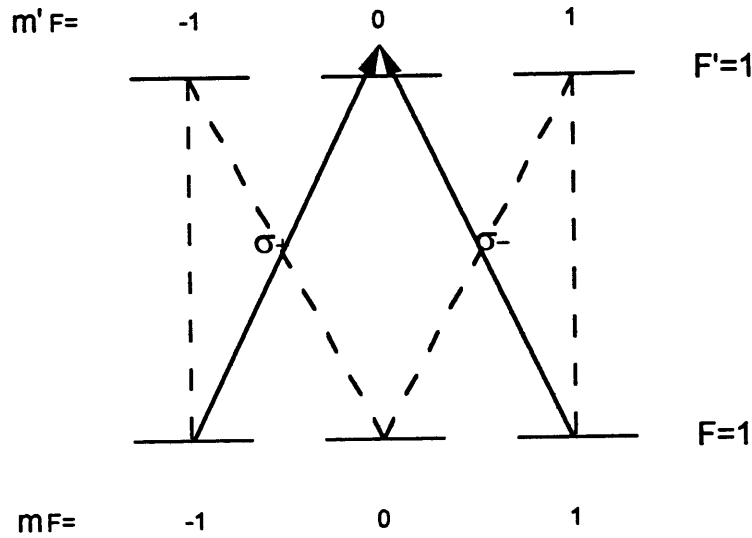


Figure 2.1: Optical pumping between two $F = 1$ states. Dashed lines represent the permitted spontaneous emissions.

explicit calculation of the Clebsh-Gordan coefficients in this case) show that the $m_F = 0 \rightarrow m'_F = 0$ transition is also forbidden. From this model, we can see that the only transitions that are going to feed the $m_F = 0$ sublevel are due to spontaneous emission from the $m'_F = \pm 1$ sublevels of the excited state. This means that after only a few cycle of optical pumping, the $m_F = 0$ sublevel is going to be depleted, and the system becomes equivalent to a simple 3-level system (Λ system as seen on figure 2.2).

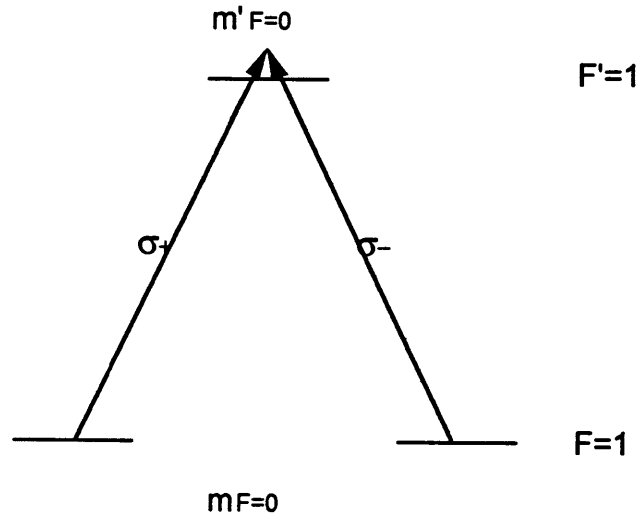


Figure 2.2: Equivalent Λ system

2.3 Coherent Population Trapping:

For simplicity, we are going to consider the Λ system presented on figure 2.3.

Here the excited state is short-lived, whereas the two ground states are long-lived. Light at frequency ω_1 couples $|a\rangle$ to $|e\rangle$, while light at ω_2 couples $|b\rangle$ to $|e\rangle$. Both couplings are electric dipole interactions, with the associated Rabi frequencies:

$g_i = \frac{\vec{\mu}_{ae} \cdot \vec{E}_i}{\hbar}$ ($i \in \{1, 2\}$), where μ is the electric dipole observable of the atom. The following detunings are defined:

$$\begin{aligned} \delta_1 &= \omega_1 - (\epsilon_e - \epsilon_a)/\hbar \\ \delta_2 &= \omega_2 - (\epsilon_e - \epsilon_b)/\hbar \\ \Delta &= \delta_1 - \delta_2 \\ \delta &= \frac{\delta_1 + \delta_2}{2} \end{aligned}$$

Finally, the individual decay rates are given by Γ_{ea} and Γ_{eb} , the total

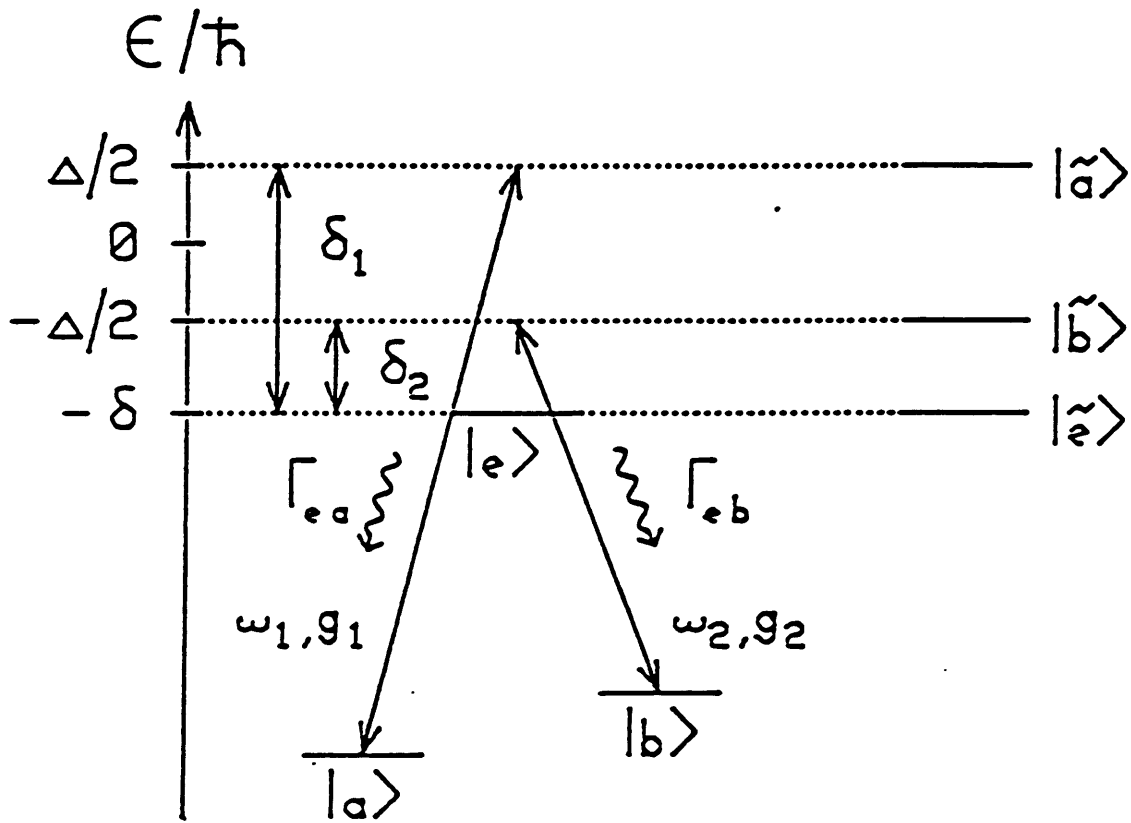


Figure 2.3: Energy diagram of a Λ system under Raman excitation. Shown are the coupling strengths and frequencies, detunings and decay rates. The states $|a\rangle, |b\rangle$ and $|e\rangle$ are the states of the atom alone. The states $|\tilde{a}\rangle, |\tilde{b}\rangle$ and $|\tilde{e}\rangle$ are the corresponding dressed states of the atom-field system.

decay rate being Γ .

Under such conditions, if we make the Rotating Wave Approximation, the Hamiltonian is:

$$H = \hbar \begin{bmatrix} \epsilon_a/\hbar & 0 & -\frac{1}{2}g_1^* e^{i\omega_1 t} \\ 0 & \epsilon_b/\hbar & -\frac{1}{2}g_2^* e^{i\omega_2 t} \\ -\frac{1}{2}g_1 e^{-i\omega_1 t} & -\frac{1}{2}g_2 e^{-i\omega_2 t} & \epsilon_e/\hbar \end{bmatrix}$$

where the three basis vectors are respectively $|a\rangle$, $|b\rangle$ and $|e\rangle$. It is then convenient to use an interacting picture, where we include the field in the system. The new state vectorial space is spanned by the new composite atom-field states:

$$|\tilde{a}\rangle = |a\rangle \otimes |\omega_1\rangle; |\tilde{b}\rangle = |b\rangle \otimes |\omega_2\rangle; |\tilde{e}\rangle = |e\rangle \otimes |0, 0, \dots\rangle$$

In that basis, the Hamiltonian transforms to:

$$\tilde{H} = \hbar \begin{bmatrix} \Delta & 0 & -g_1^* \\ 0 & -\Delta & -g_2^* \\ -g_1 & -g_2 & (-2\delta - i\Gamma) \end{bmatrix},$$

where we have chosen the origin of energy so that: $\delta + \epsilon_e = 0$. We have also introduced the damping rate to account for spontaneous emission. A diagram of the new energy levels is illustrated on figure 2.3. The evolution of the density matrix of the system is given by:

$$\dot{\tilde{\rho}} = \frac{i}{\hbar} [\tilde{\rho}\tilde{H}^\dagger - \tilde{H}\tilde{\rho}] + \tilde{L}\tilde{\rho}\tilde{e}\tilde{e}, \text{ where } \tilde{L} \text{ is the source matrix:}$$

$$\tilde{L} = \begin{bmatrix} \Gamma_{ea} & 0 & 0 \\ 0 & \Gamma_{eb} & 0 \\ 0 & 0 & 0 \end{bmatrix}$$

The Raman interaction can be more easily understood if we use another basis: $|- \rangle = \cos\theta|\tilde{a}\rangle - \sin\theta|\tilde{b}\rangle$; $|+ \rangle = \cos\theta|\tilde{a}\rangle + \sin\theta|\tilde{b}\rangle$; $|e\rangle = |\tilde{e}\rangle$, where:

$$\begin{aligned} \sin\theta &= \frac{g_1}{g} \\ \cos\theta &= \frac{g_2}{g} \\ g &= \sqrt{g_1^2 + g_2^2} \end{aligned}$$

This is in fact a simple rotation in the space spanned by the two ground states.

$$H = \frac{\hbar}{2} \begin{bmatrix} C\Delta & S\Delta & 0 \\ S\Delta & -C\Delta & -g \\ 0 & -g & -2\delta - i\Gamma \end{bmatrix},$$

where $C = \cos 2\theta$ and $S = \sin 2\theta$, and the transformed source matrix is:

$$\tilde{L} = \frac{\Gamma}{2} \begin{bmatrix} 1 + Cd & Sd & 0 \\ Sd & 1 - Cd & 0 \\ 0 & 0 & 0 \end{bmatrix},$$

where: $d = (\Gamma_{ea} - \Gamma_{eb})/\Gamma$

The essential result here is that the $|-\rangle$ state is decoupled from the excited state, it doesn't see any absorption, which is why it's often called *dark state*. If all atoms can be prepared in the dark state, the system will be transparent.

Coherent Population Trapping is the process that can be used to obtain such a state. Let's consider the following conditions:

- $\Delta = 0$
- $d = 0$

Under such conditions, the dark state and the $|+\rangle$ state are uncoupled to each other directly, the $|+\rangle$ state is coupled with the excited state with a Rabi frequency of g and the excited states relaxes equally with a rate $\Gamma/2$ to the dark state and to the $|+\rangle$ state (cf figure 2.4).

It is then obvious that soon all the atoms are going to be trapped in the dark state, so that the system becomes totally transparent. This is what explains the so called 'Raman dip' that happens for $\Delta = 0$.

Actually under the following assumptions: $|g_1| = |g_2| = g$,
 $d = 0$,

$|\Delta|, |\delta| \ll g \ll \Gamma$, the excited state population is given by:

$$\rho_{ee} = \frac{g^2 \Delta^2}{g^4 + g^2 \Delta^2 + \Delta^2 \Gamma^2 + 4\delta^2 \Delta^2 + \Delta^4},$$

This expression can be simplified with our assumptions to:

$$\rho_{ee} = \frac{g^2/\Gamma}{\Gamma} \frac{\Delta^2}{\Delta^2 + (g^2/\Gamma)^2},$$

which explains the absorption profile shown on figure 2.5.

The explanation of the narrow width of the CPT effect is given by the fact that for non zero detuning, the dark state and the $|+\rangle$ state are coupled together, so that a $|-\rangle$ state evolves into $|+\rangle$ after a time π/Δ , if

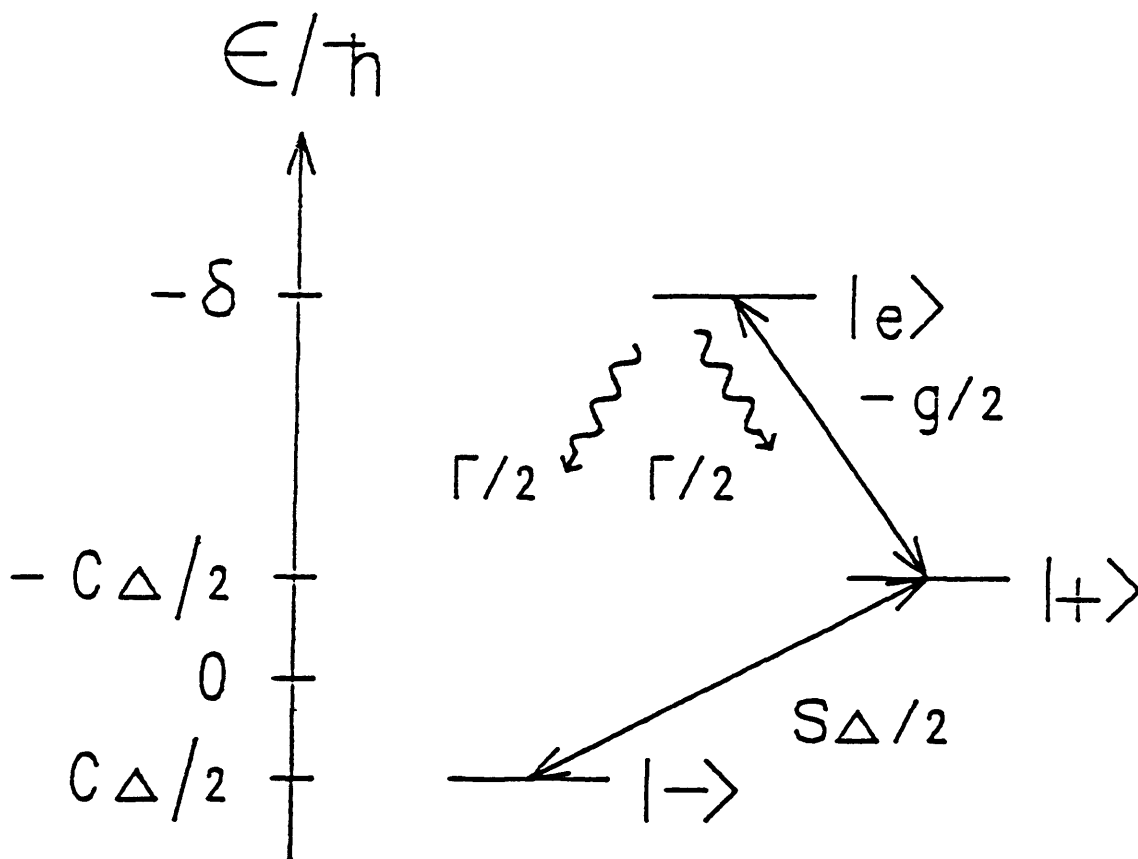


Figure 2.4: Coherent Population Trapping

we neglect field coupling and consider $g_1 = g_2$. This coupling explains why CPT disappears when Δ gets big enough (eg CPT reduces to half when $\Delta = g^2/\Lambda$).

It is interesting to see, here, that there are two easy ways to control Δ :

- By simply tuning one of the two frequencies,
- By using Zeeman shift of a sublevel of an hyperfine manifold, as seen previously.

Finally, under the assumption of strong non depleted forward and probe fields, and resonance ($\Delta = 0$), one can show that the coherence between the

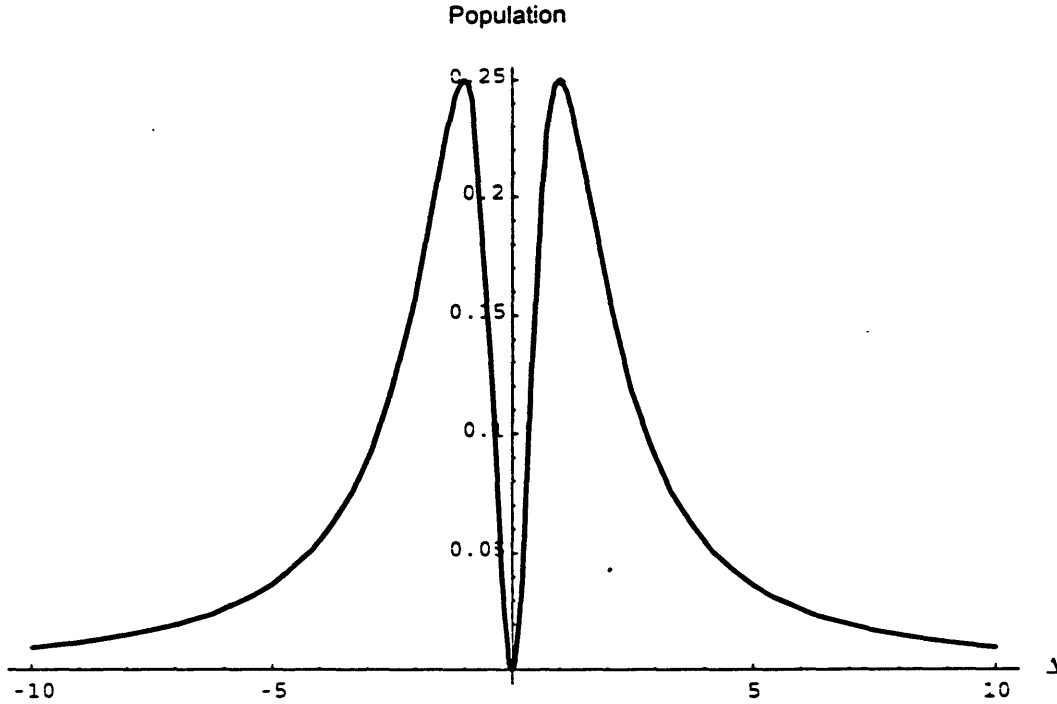


Figure 2.5: Raman dip ($g = \Gamma$, Δ in units of Γ)

$|a\rangle$ and $|b\rangle$ states is given by:

$$\rho_{ab} = -\frac{g_P g_F^*}{g^2} e^{i(\vec{k}_P - \vec{k}_F) \cdot \vec{r}},$$

when optical pumping is achieved. This shows a purely sinusoidal phase grating in the coherence between the two ground states, without any ground state population grating. This result is corroborated by a more complete treatment [3] that shows that under the only assumption of low power probe, in a first order development, this phase grating still exists.

2.4 Application to OPC:

2.4.1 Advantages of CPT:

Classical nonlinear optics deal with field frequencies that are far from any resonance, and can be well treated by an expansion of the polarization in a power series of the incident fields amplitudes.

Going near resonance brings stronger coupling between the fields and the medium, a priori improving the nonlinear effects, but the resonant non-linearity cannot be treated anymore by an expansion. Instead, it arises from

the saturation of the transition. For a two level atoms vapor, this means that the whole Doppler profile has to be saturated, and to make it worse, the two level absorption kills the gain, requiring even more intensity.

We know however that the Raman two photon transition ($\Delta = 0$) is saturated at arbitrarily low power¹, since saturation of the Λ system corresponds to optical pumping into the dark the state.

This is actually the essential feature of CPT, because it means that OPC can be obtained with no real constraint on the intensity. The consequence is that CPT brings more freedom than for a regular two level system, and this can be used to make a trade off between power and response time. Indeed the response time is inversely proportional to the optical pumping rate that goes as g^2/Γ . Thus since we know that for a two level system, when saturation is obtained ($g \approx \Gamma$), the response time $1/\Gamma$ is of the order of 10 ns, we know that for an intensity 100 times lower than the two level saturation intensity, we'll get a response time of $1\mu s$.

In short, CPT allows us to relax the constraint on the response time in favor of a lower power requirement, so that we can meet the specifications needed by practical applications.

2.4.2 Chosen Configuration:

The tuning of the different fields is shown on figure 2.6.

The fields have to be resonant, but if they are too close to resonance, absorption will soon be predominant and overcome the gain in efficiency. A trade off has to be made between resonance and absorption, from a doppler profile of width around 1 GHz, we chose to tune the fields on the tail of the profile, blue-shifted of about 200 to 500 MHz (δ_1 on the figure).

To obtain some Raman gain, the ground state interacting with the forward field has to be more populated than the other ground state. This is obtained by making the backward field more resonant than the forward field.

We want to avoid the formation of a dark state due to the forward and backward field, so we chose to detune the forward beam from the backward beam by 60 to 100 MHz (δ_2 on the figure).

Finally, we can remark that the grating that corresponds to the interference backward/probe won't exist. Indeed, its amplitude is proportional to the real part of $\vec{E}_B \cdot \vec{E}_F^*$, which is null since the two beams have the same circular polarization.

¹Actually the coherence decay rate γ_{ab} implies a low threshold: $g \geq \sqrt{\Gamma\gamma_{ab}}$.

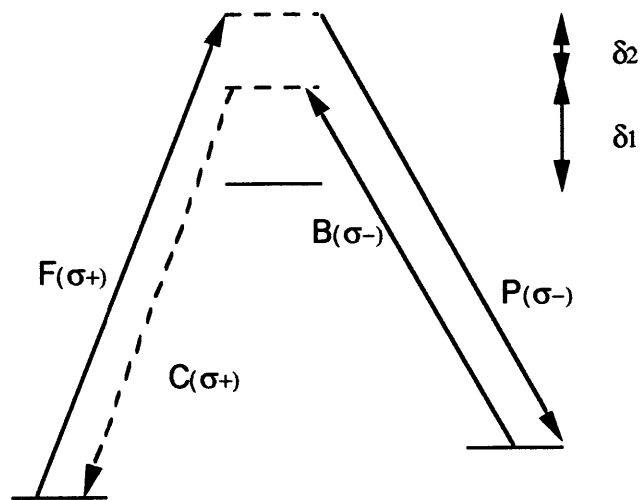


Figure 2.6: Fields configuration.

Chapter 3

Experimental Setup:

3.1 Main issues:

Following the previous analysis, we already have a set of well identified constraints to achieve OPC in a rubidium vapor. Furthermore practical considerations bring their own constraints that have to be identified before considering the final design.

3.1.1 Optical System:

Frequencies:

The first issue is the frequency of the beams. Since we decided to work on hyperfine level of rubidium, the frequencies can all be obtained by shifting with acousto-optic modulators of a main laser beam. Even if it would be possible to use two different lasers, the availability of a frequency stabilized titanium:sapphire laser lead to the choice of a single laser. Since this laser has a very good stability, the first issue was to be able to lock it to a particular frequency inside the D1 transition of rubidium. To be able to do so, a saturable absorption setup was used (cf figure 3.1 (a)).

The idea of saturable absorption is to use saturation of absorption to be able to discern the atomic transitions in the doppler profile. An unsaturated beam is used to measure the Doppler profile. A ‘strong’ beam is aligned with another probe beam, but counterpropagating. The saturation beam interacts with atoms whose velocity bring them within the linewidth of the absorption of a given line, and burns a spectral hole at its frequency in the doppler profile of the line (cf figure 3.1(b)). Since the ‘pump’ and the probe are counterpropagating the probe beam sees an absorption profile that is obtained by flipping the ‘burnt’ profile generated by the pump around its central frequency (the velocities are opposite, the doppler shift is then also opposite). That’s why the probe is represented as having a frequency which is symmetrical around the central frequency.

If the frequency of the laser is right on an absorption line, the probe beam and the saturating beam are going to interact with the same class of atoms, ie the ones at zero velocity. To see it in a more mathematical way, we can write that atoms that ‘see’ the pump have a longitudinal velocity v such as:

$$f_0 = f_L(1 - \frac{v}{c}),$$

whereas the probe talks with atoms that have the opposite velocity.

By subtracting the intensities of the two probe beams, it is possible to detect clearly when this happens by measuring the decrease of absorption due to the saturation, with a narrow linewidth.

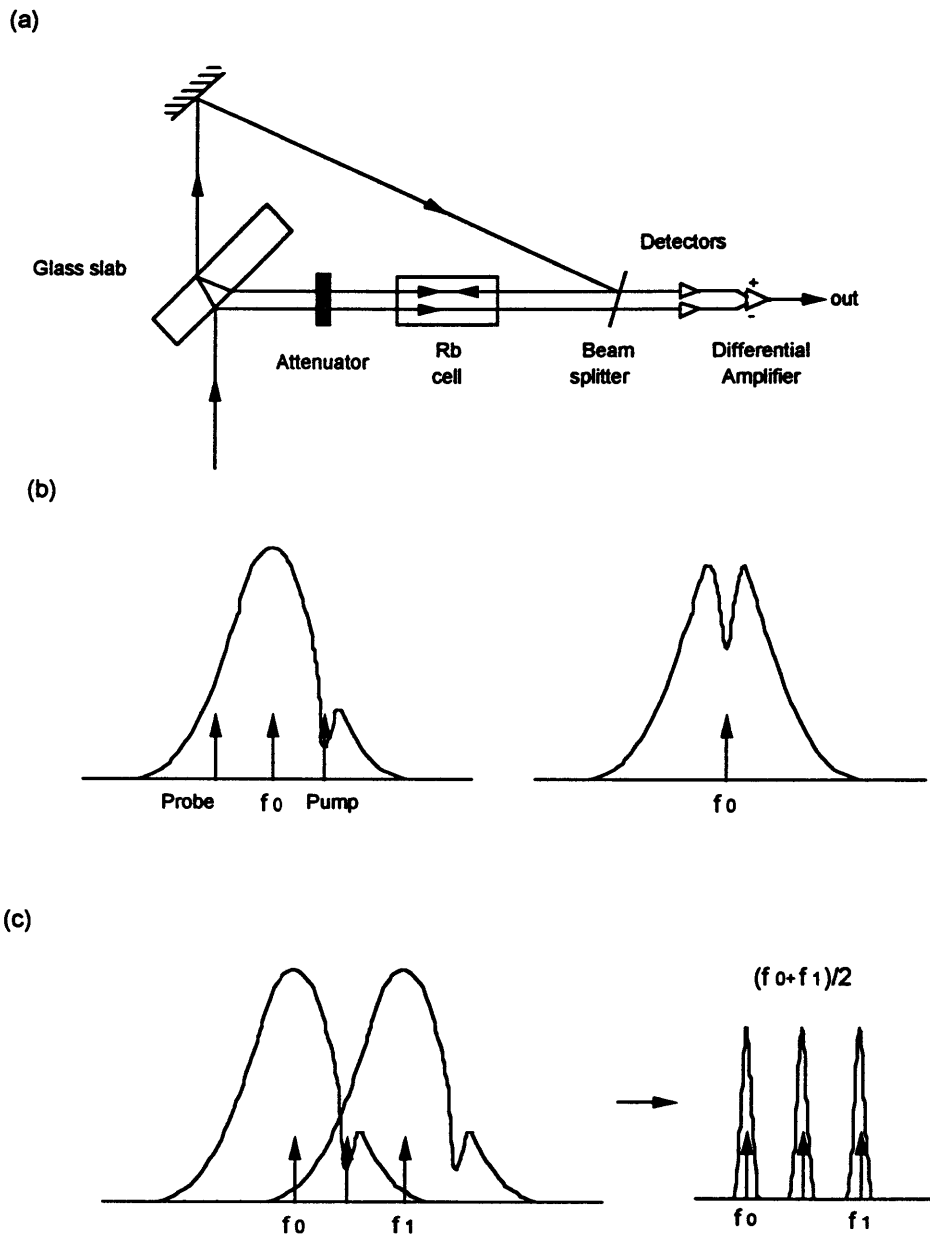


Figure 3.1: (a) Saturated absorption setup (b) Spectral hole burning (c) Crossover effect

A side-effect of this method is that a peak (a ‘crossover’) is also detected when the laser frequency stands right in the middle of two absorption line (cf figure 3.1). Indeed when this happens for the low frequency line (around f_0), atoms that see the pump and get into the excited state have the velocity v such that:

$$f_0 = f_L(1 - \frac{v}{c})$$

Now if you consider absorption of the probe, on the high frequency line (around f_1), some atoms are going to be in the excited state if:

$$f_1 = f_L(1 + \frac{v}{c})$$

The probe is going to see less absorption, since a part of the population is already excited by the pump (for the other line). A crossover happens when:

$$\frac{f_0}{(1-\frac{v}{c})} = \frac{f_1}{(1+\frac{v}{c})}$$

$$\frac{v}{c} = 1 - \frac{f_0}{f_L} = \frac{f_1}{f_L} - 1$$

Which is obtained when the laser frequency is:

$$f_L = \frac{f_0+f_1}{2}$$

Crossovers are actually no problem, and this feature can in fact even be useful as far as identification of a line is involved, or even can be used to lock the laser in the middle of two lines.

The limitations of the linewidth are given by:

- The natural inhomogeneous linewidth of the transition,
- The jitter of the laser,
- The transit time of an atom that has a non-zero transverse velocity (ie atoms don’t stay forever in the beam),
- Power broadening,
- Collisional broadening.

To get the best conditions, the setup was used with as low a power as possible (avoiding power broadening) and low temperature (for collisional broadening). For transit time, a trade-off has to be made between intensity and size of the beam, since saturation increases with intensity, whereas transit time increases with the size of the beams. The setup used gave a 9 MHz linewidth. The natural linewidth of rubidium is around 5.8 MHz, measurement showed that the laser width is 2 MHz. The resulting linewidth is possibly attributable to residual power broadening, transit time broadening or measurement error. The differential amplifier that was used is described

on figure 3.2. The frequency of the two pumps is easily obtained by shifting

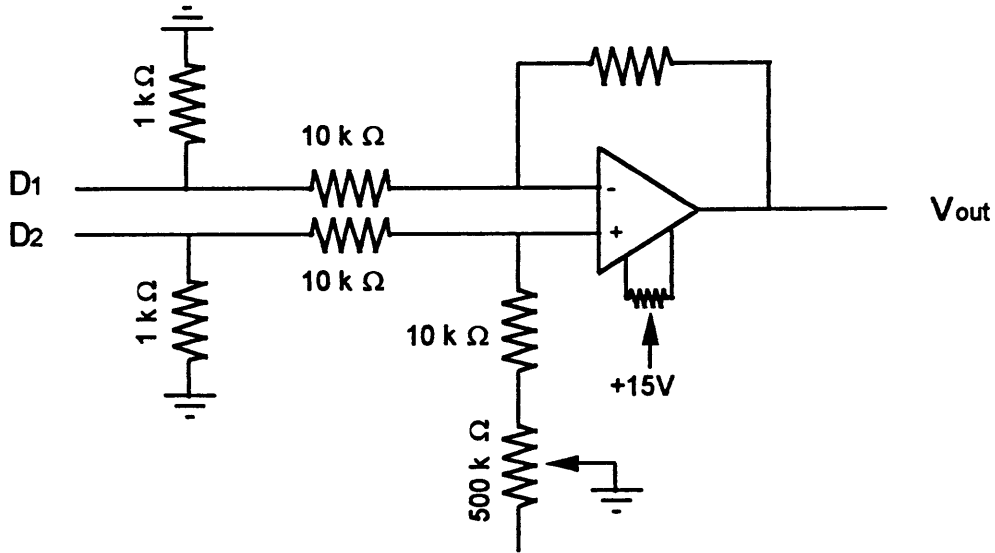


Figure 3.2: Differential amplifier used for the saturable absorption setup.

with two acousto-optics modulator. Since the idea was to use CPT with Zeeman hyperfine sublevels, the probe beam had to be close in frequency to the forward beam. This has been obtained by shifting the frequency of a fraction of the forward beam with a back-to-back AOMs setup (cf figure 3.3). The principle is to use two AOMs shifting in opposite directions in frequency, in a way that preserve the alignment of the beam as much as possible. This can be achieved if the two AOMs have opposite orientation. Let's call θ_1 and θ_2 the two deflections due to the AOMs, Δf_1 and Δf_2 the two frequency shifts. Since the momentum change due to the acoustic waves is very small, we have a proportionality between shift and deflection:

$$\begin{aligned}\theta_1 &= \alpha \Delta f_1, \\ \theta_2 &= -\alpha \Delta f_2,\end{aligned}$$

the change of sign being due to the opposite orientations of the AOMs. The total effect is then:

$$\theta = \alpha(\Delta f_1 - \Delta f_2)$$

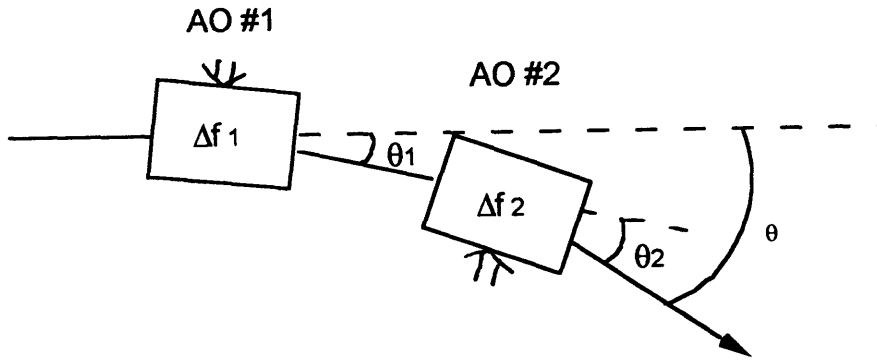


Figure 3.3: Back-to-back AOMs setup

$$\Delta f = \Delta f_1 + \Delta f_2$$

This makes possible the frequency shift of the beams without deflection, the only effect being a slight translation of the beam due to the propagation between the two AOMs, the condition being:

$$\Delta f_1 - \Delta f_2 = \text{Constant}$$

This relationship can be maintained by use of a circuit that has been designed to control the two RF generators used to supply the AOMs (cf figure 3.4). The principle of this circuit is to supply two voltages to the RF generators calculated to provide the appropriate shifts, in a linearization around the 0 frequency.

Finally, a simple control box has been designed which provides a remote control of the laser frequency ('external' scanning) and of the shift-frequencies of the two main AOMs. This circuit is simply a set of 3 voltage followers as the one seen on figure 3.5.

Geometrical Configuration:

The counterpropagative configuration could have been used, but is source of many problems like risk of feedback to the laser, difficulty to pick up the conjugate and to measure intensities. Thus, since phase-matching is not a constraint, the following geometry has been chosen: The two pumps were sized with telescopes to correspond to beams focused in the middle of the cell, with a FWHM radius of approximately 1 mm, whereas the probe was chosen to be 0.7 mm FWHM at the same point.

Rough alignment of the beams was achieved by positioning the beams spot on a square of 5 mm side on two mirrors placed 97 cm apart symmetrically

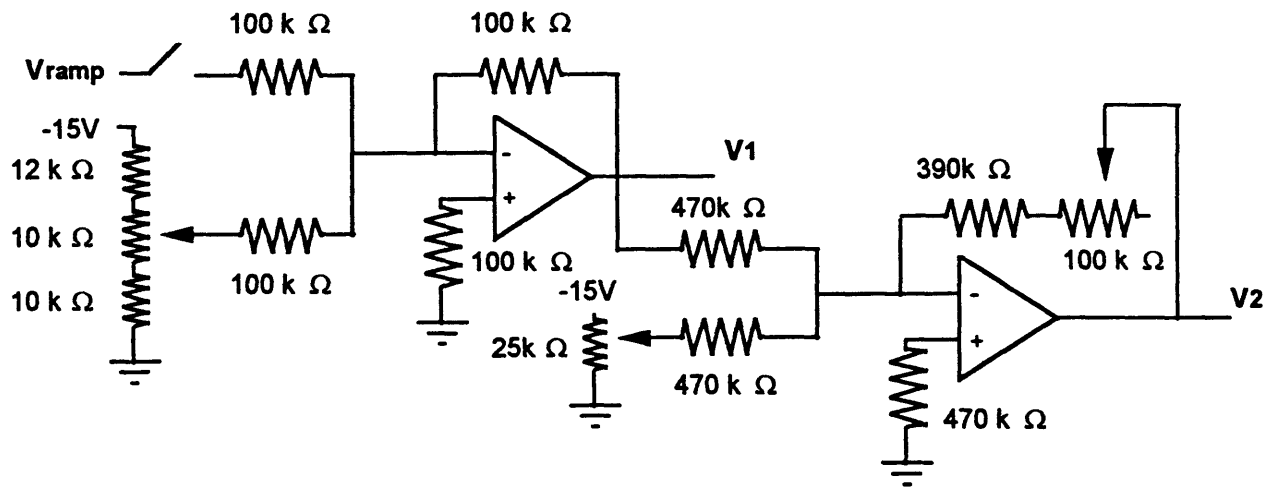


Figure 3.4: Control circuit of the RF drivers

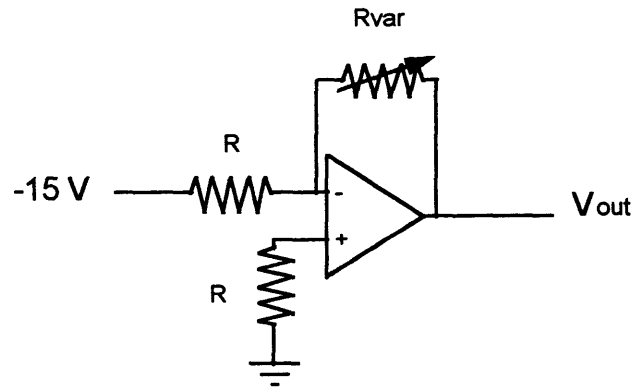
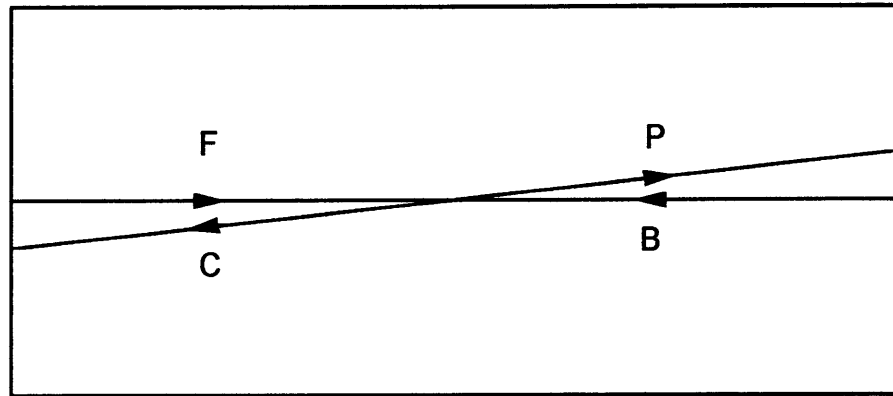


Figure 3.5: Frequency control circuit

(a)



(b)

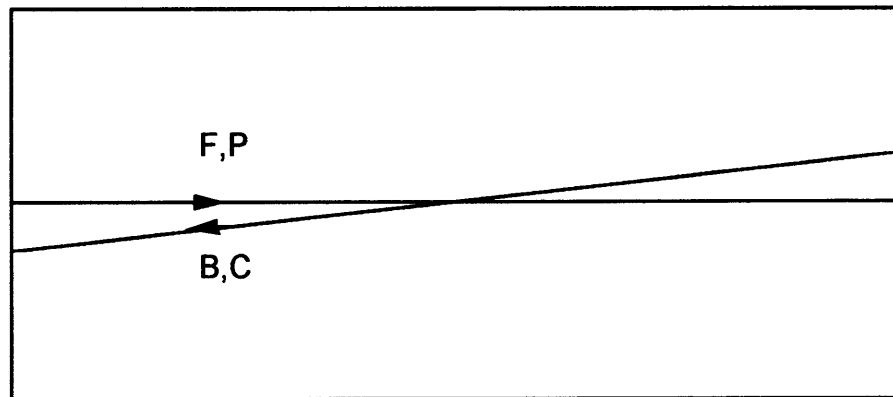


Figure 3.6: (a) View in a vertical plan (b) View in a horizontal plan

on each side of the cell.

Polarizations:

To choose an orientation for the system, the polarization of the forward pump has been arbitrarily chosen to be σ_+ . From this choice, the probe and backward beams have to be σ_- , whereas the conjugate will be σ_+ . To preserve the quality of the polarizations, an important issue is to minimize the number of reflections after the polarization of the laser light. Indeed, any mirror (with a non-normal incidence) will reflect two perpendicular polarizations in a different way. Without precaution, a circular polarization becomes quickly elliptical (that is, combination of σ_+ and σ_-). Even a linear polarization will become elliptical.

Following this idea, the final design has been made so that any beam is polarized in three steps, as close as possible to the input windows of the cell in term of number of reflections:

- The polarization of the beam is rotated by a half-wave plate,
- The beam goes through a linear-polarization element, that has been chosen to be a polarization cube, which provides easy access to either polarization,
- The linearly polarized beam goes through a quarter-wave plate orientated so that the output is circularly polarized.

3.1.2 Atomic Vapor:

The OPC element being atomic rubidium, it is necessary to have a good way to create an atomic vapor of this element. The solution is to use a cell put under vacuum that can be easily heated and provides optical access to the beams. Under such conditions, the easy solution seems to be the use of a simple glass cell, but it's unfortunately not possible since the relatively cold surface of the cell would be quickly covered by a thin layer of metallic rubidium, blocking optical access. The best solution is in fact the use of a heat-pipe oven. This device is described in figure 3.7. The oven is basically constituted by two perpendicular pipes soldered together:

- The reservoir of metallic rubidium,
- The interacting region container, perpendicular to the reservoir,

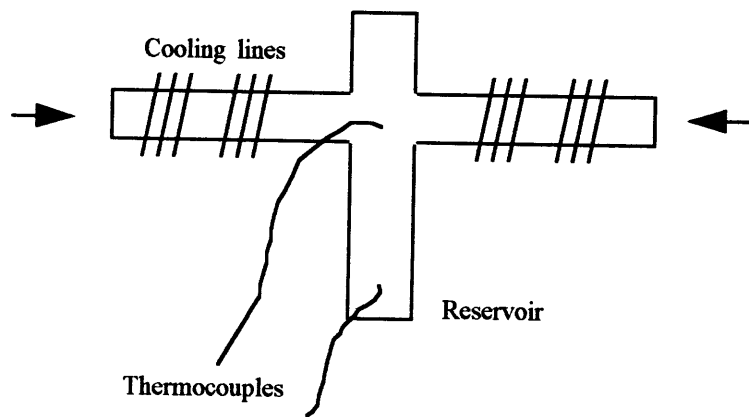


Figure 3.7: Heat-pipe oven design

The reservoir is provided with its own heating system. Since rubidium has a low melting temperature (38°C under atmospheric pressure), only mild heating is required (heating tape). The interaction region is set to be in the center of the cell, at the cross between the two pipes. Heavy heating is required to get a high enough vapor density at this point, which is provided by a set of heating coils. To contain the vapor inside the interaction region, and protect the optical windows from being coated, two sets of cooling water pipes are wrapped around both ends of the cell. The temperature is monitored with two thermocouples put at the cross and at the reservoir.

An important issue is magnetic perturbation. Since we're using hyperfine Zeeman sub-levels, it is of great importance to have no unwanted magnetic field in the interaction region. This is achieved with a magnetic shielding of mu-metal, and by using twisted pairs of Nichrome and copper to avoid generation of magnetic field by the cross heating system. Following the same concern, the thermocouples are made with twisted pairs also. Furthermore a set of Helmholtz coils was made to be able to scan the Zeeman detuning of the $m = \pm 1$ states. Those coils are constituted by 95 turns of copper wire (diameter .053"), on a bakelite cylinder of diameter 3.068". These coils produce a magnetic field of 8.33 Gauss per Ampere of current, for a spacing of four inches. A circuit has been designed to provide a current source, with a scanning feature (cf figure 3.8). With proper load, 1.31 V of monitor voltage corresponds to one Ampere of current, when the scanning feature is used.

Vacuum is simply obtained with a mechanical pump, the only concern being that rubidium is extremely reactive (it explodes to the contact of water). Great care has thus been taken to obtain a leak-free system, leaks being detected by spraying acetone on all the potential leak regions (acetone has a low vapor pressure and creates a sudden increase of pressure when sprayed on a leak).

3.2 Design of the System:

3.2.1 Optics:

A simplified scheme of the setup is presented in figure 3.9. This scheme doesn't include:

- The telescopes used to size the beams,
- The lenses put on each side of each AOM used to focus the beams,

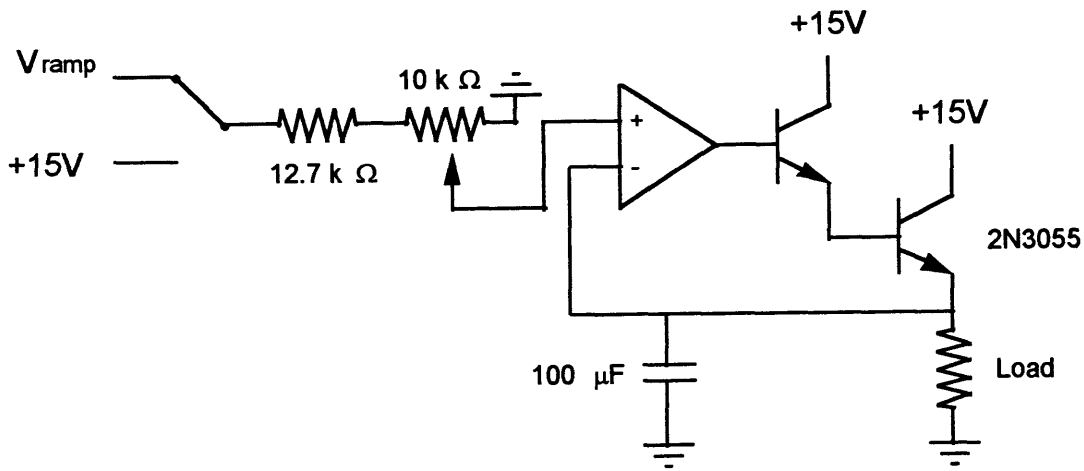


Figure 3.8: Current source circuit

- The collecting optics (98% beamsplitters and closely spaced mirrors).

The real system also includes supplementary mirrors used to form the particular geometry chosen (couple of mirrors used to position the beams).

The conjugate beam is collected along the probe path. Indeed it has the opposite circular polarization than the probe, but it goes through the other side of the quarterwave plate, so that it has the linear polarization corresponding to the one that has the probe before it is made circular.

The amplified probe is similarly reflected by the polarization splitter on the backward side, and can be also measured.

The two pumps are simply measured after transmission through two 98% beamsplitters put on each side on the cell, 97 cm apart.

3.2.2 Vapor Cell:

The cell is presented in figure 3.10 and the water cooling system in figure 3.11. The heating systems is constituted by:

- A heating tape around the reservoir, outside the magnetic shield,
- A twisted pair of copper and nichrome, with 3 layers on the cross and 1 everywhere else.

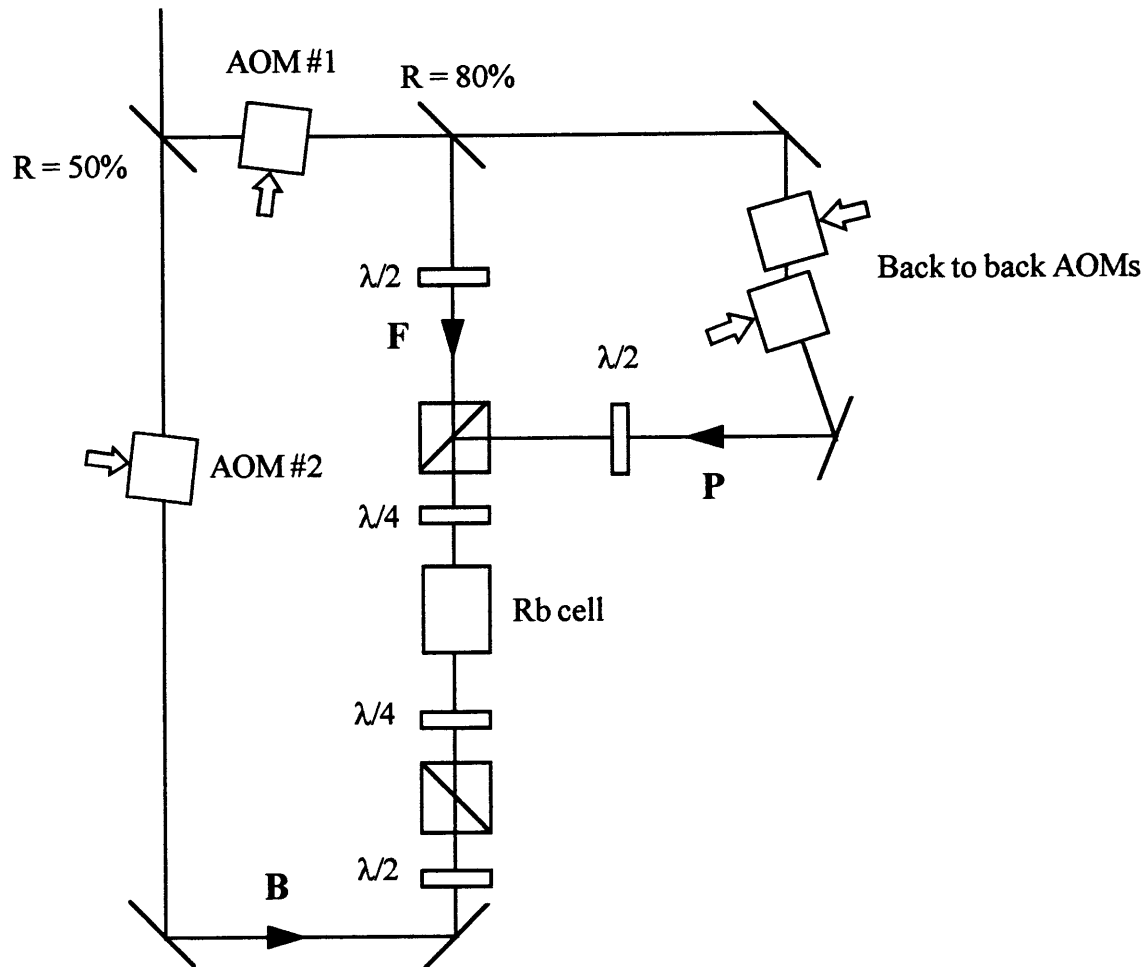


Figure 3.9: Simplified optical setup

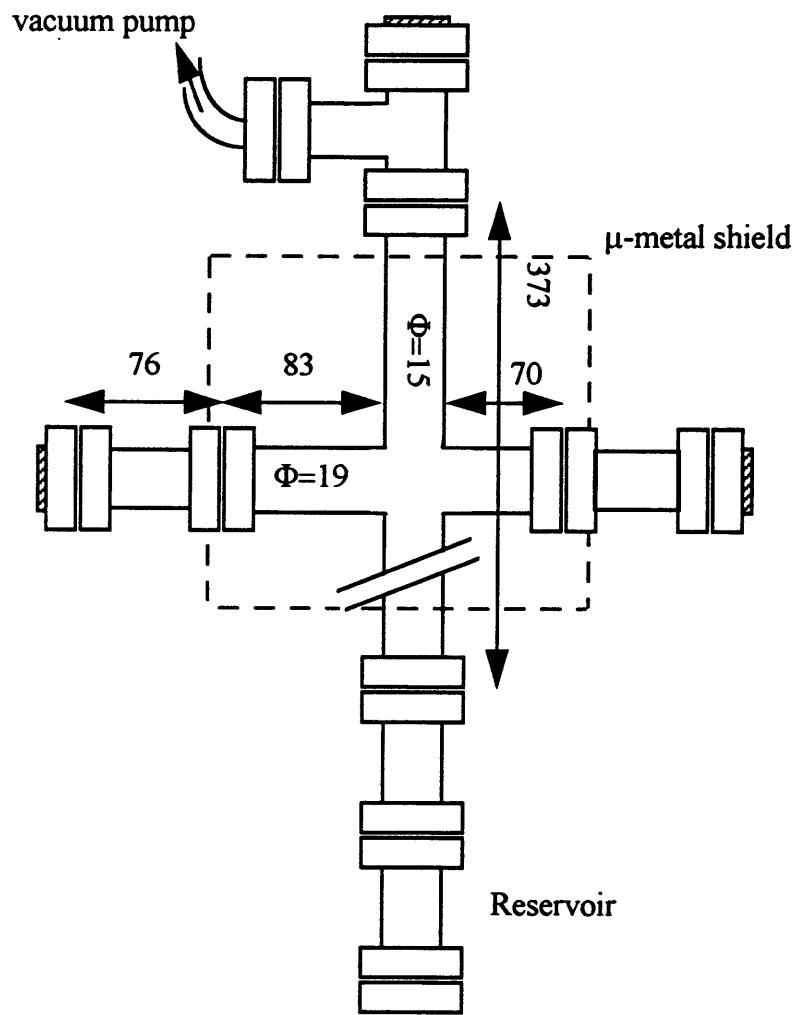


Figure 3.10: The vapor cell used in the experiment (dimensions in mm).

Each heating system is supplied by a variac, and temperature is monitored with two thermocouples, one on the central point of the cross, the other one on the bottom of the reservoir.

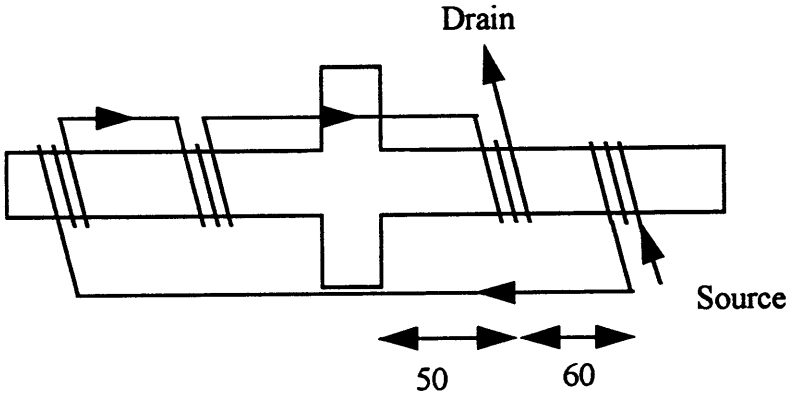


Figure 3.11: Cooling setup (dimensions in mm).

Chapter 4

Results:

4.1 Characterization:

Once the polarization was correctly set, OPC was quite easily achieved. The conjugate beam appeared as a slightly bigger spot than the pumps (around 1.5 mm), propagating in the direction imposed by phase matching.

4.1.1 Experimental Conditions:

The results presented in this section were obtained with the following conditions:

- Forward beam upshifted by 318.35 MHz, power of 14 mW,
- Backward beam upshifted by 237.38 MHz, power of 8 mW,
- Probe beam upshifted of 316.51 MHz, power of $660\mu W$,
- Magnetic field of 1.54 Gauss,
- Temperature of the reservoir of $215^{\circ}C$,
- Temperature of the cross of $142^{\circ}C$.

Saturable Absorption:

Figure 4.1 presents the result obtained with the saturable absorption setup on the D1 lines of rubidium. This result has been used in all the following experiments as a reference for all the frequencies measurements. The corresponding transitions are identified, as well as the concerned isotope. The presence of crossovers in the middle of each pairs of close lines can be seen clearly.

Overview:

Figure 4.2 shows the reflectivity obtained, for the lines corresponding to the $F=2$ ground state of ^{87}Rb and $F=3$ ground state of ^{85}Rb . This range of frequency has been indeed been found to provide the biggest reflectivity, and as such was chosen as object of the following studies, keeping in mind that high reflectivity is an important issue as far as applications are concerned. Furthermore the most efficient line has been found to correspond to the $F = 2 \rightarrow F' = 1$ line (^{87}Rb), which will be particularly studied.

Figure 4.3 shows the power of the outgoing probe versus the frequency of the laser. We can see that generation of the conjugate corresponds also

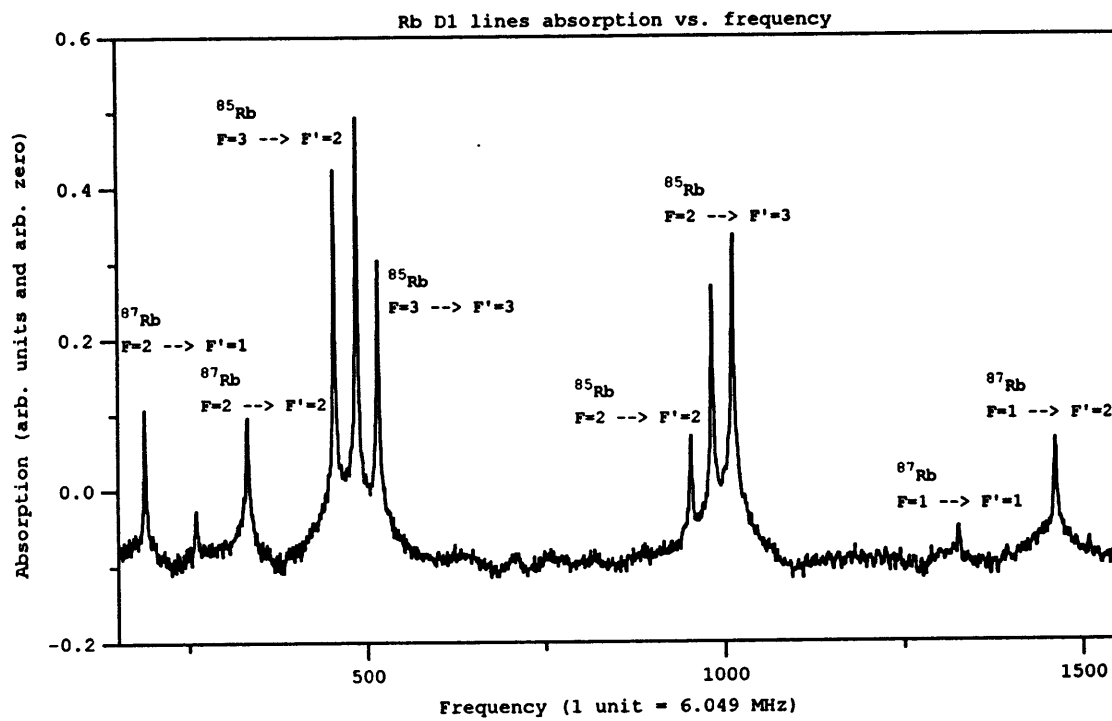


Figure 4.1: Rb D1 absorption lines versus frequency (1 unit is 6.049 MHz).

to amplification of the probe (its power goes slightly above $660\mu W$). A lot more gain was seen under conditions reported later on.

Polarization Issue:

Figure 4.4 shows the power measured on each polarization of the conjugate. This measurement can be easily done, since after crossing the quarter waveplate, each circular polarization is transformed into one linear polarization that corresponds to one of the two polarization axis of the polarization splitter. The unit is chosen so that the maximum power corresponds to 1. It is obvious that power corresponding to the polarization opposite to the one we predict is extremely low (.6 %!!). This means that the conjugate is in practice circular (σ_+ polarization according to our convention).

Figure 4.5 shows the ratio of the power with the correct polarization to the total power, this always stays close to 1.

4.1.2 CPT Diagnostic:

As we saw during our study of CPT, the linewidth of the CPT effect can be extremely low (going like g^2/Γ). When conjugation is due to a two-level system, the linewidth of the effect is found to be approximately the natural linewidth, plus power-broadening. So if we can prove that we obtained subnatural linewidth, this will make sure that we really observed a CPT mediated conjugation. As we pointed it out, we have two ways of detuning the probe. This gives two independent measurements. These two ways have been tried on the $F = 2 \rightarrow F' = 1$ transition of ^{87}Rb .

Zeeman Shift Tuning:

This is the simplest way, since it only requires to scan the magnetic field amplitude. The corresponding two-photon detuning, using the Landé factor is found to be 1.40 MHz for each Gauss of applied magnetic field. The result is shown on figure 4.6. The FWHM linewidth is measured to be of 2.4 MHz, which is well below the natural linewidth (5.8 MHz). This is absolutely consistent with our proposed mechanism.

Probe Tuning:

The back-to-back AOMs setup provides us a way of simply tuning the probe frequency. Unfortunately, it has been found that the AOMs used have a low bandwidth when they're used in a fixed configuration. However we can get

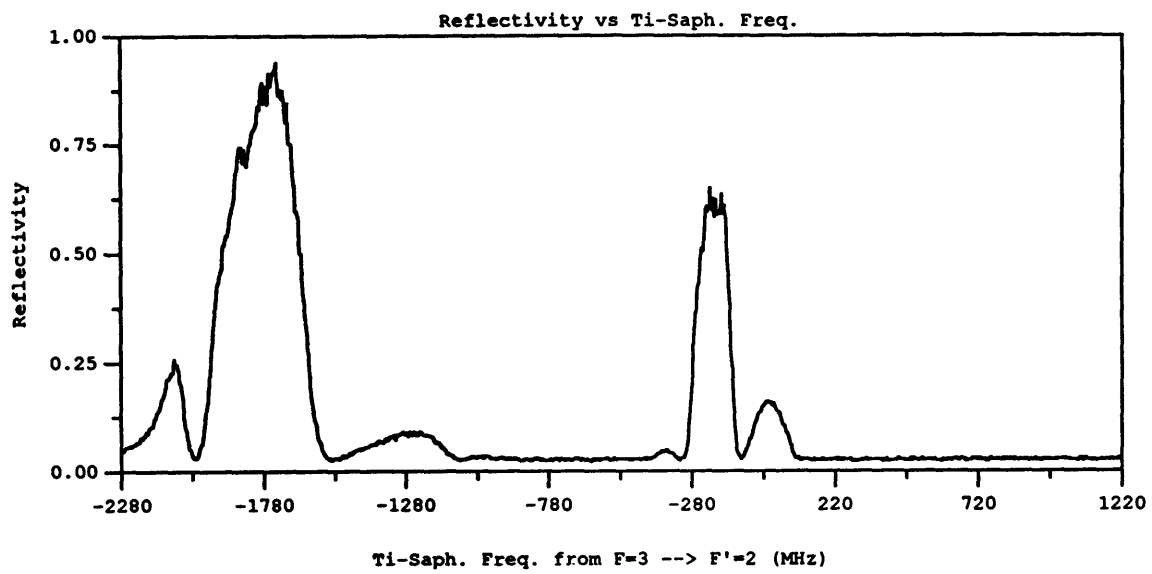


Figure 4.2: Reflectivity of the conjugate versus frequency (MHz).

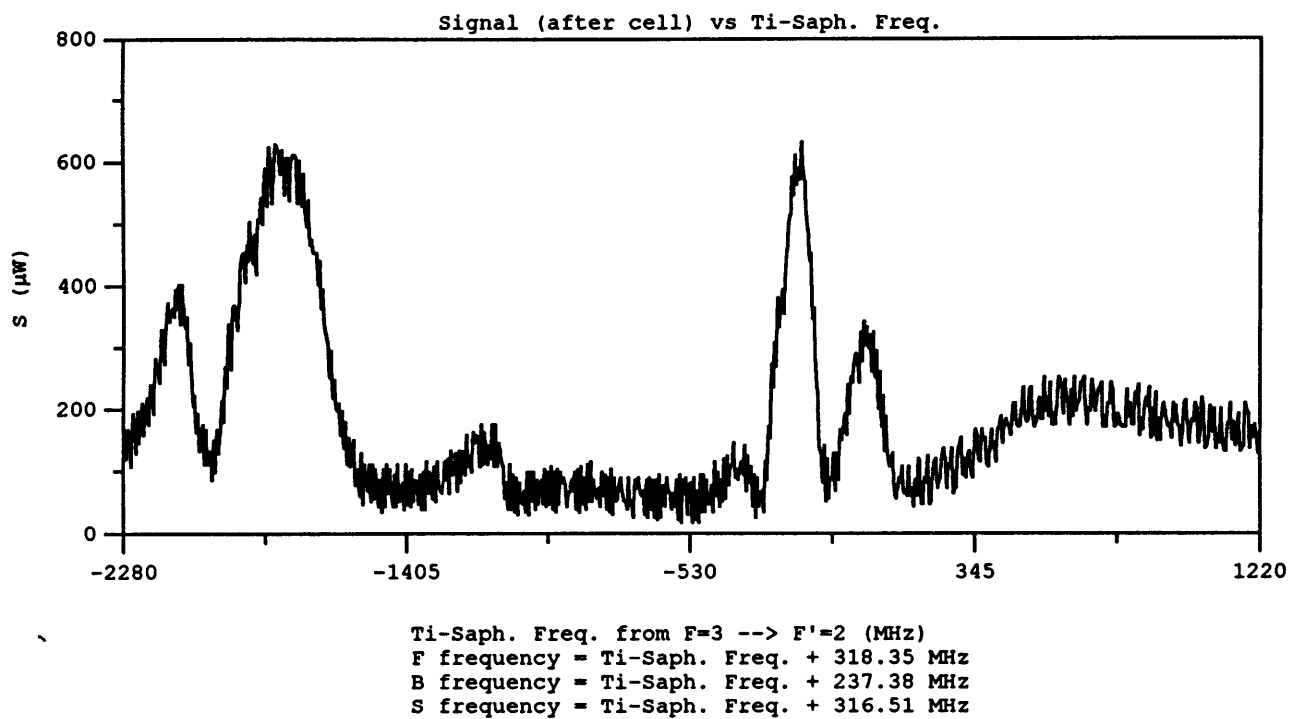
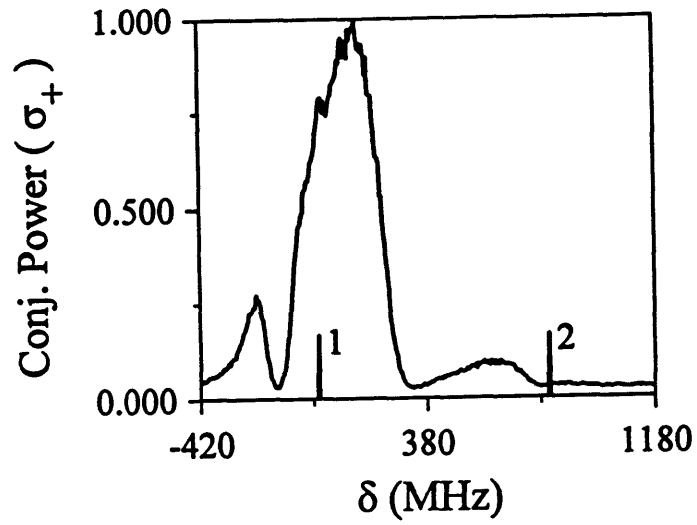


Figure 4.3: Amplified probe power versus frequency (MHz).

(a)



(b)

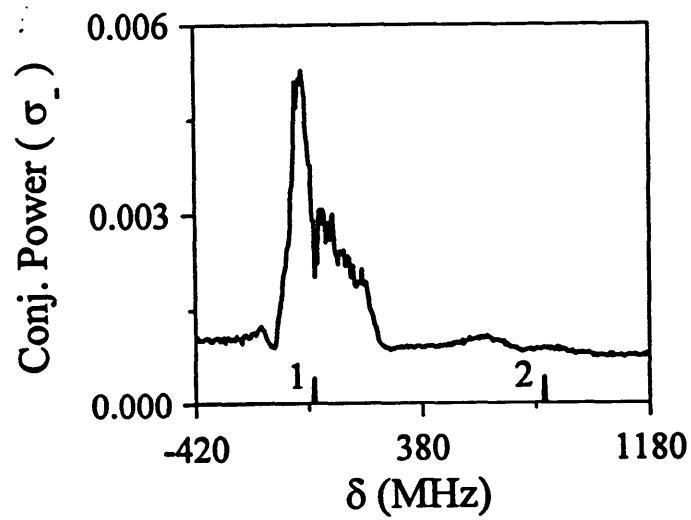


Figure 4.4: (a) Power of the conjugate with the predicted polarization (b) Power of the conjugate with the opposite polarization.

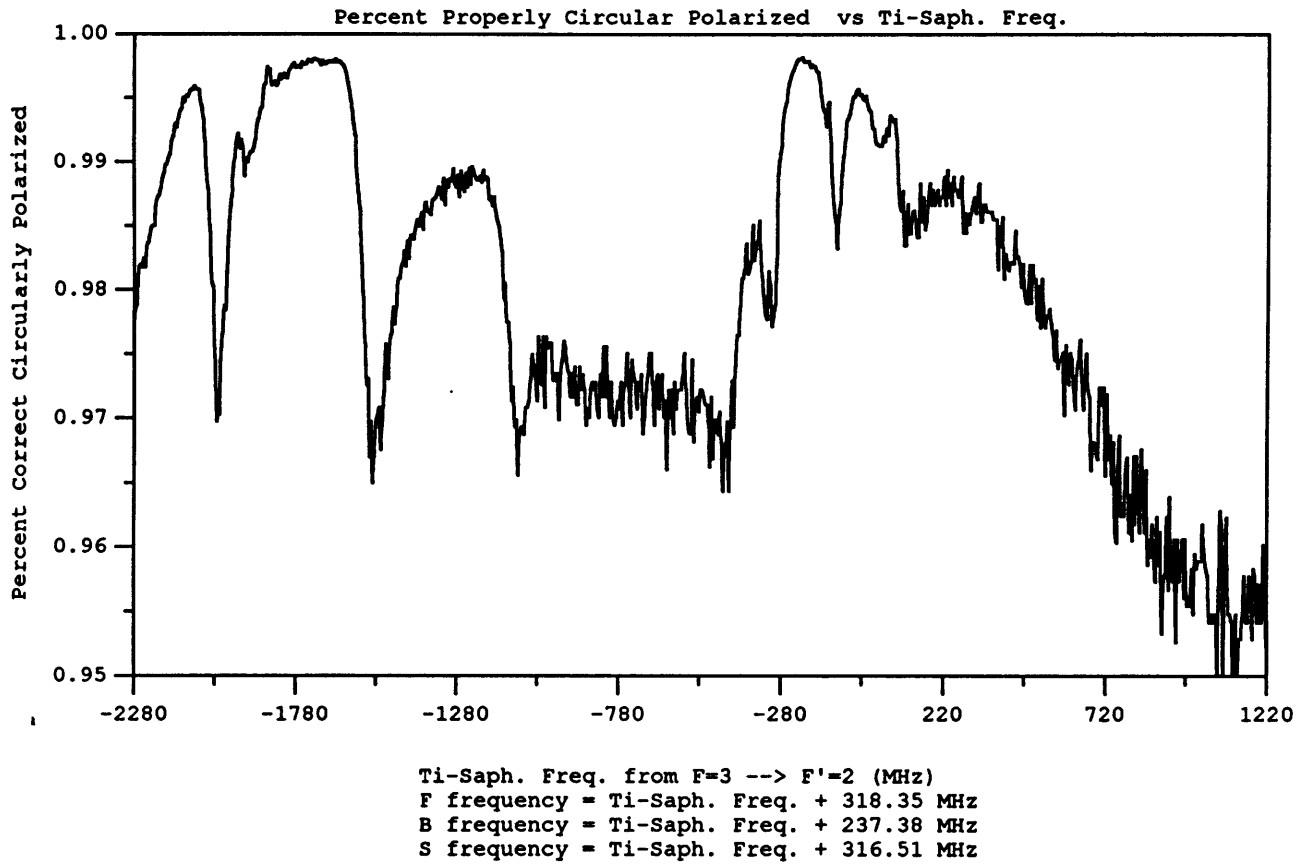


Figure 4.5: Fraction of the conjugate having the correct polarization.

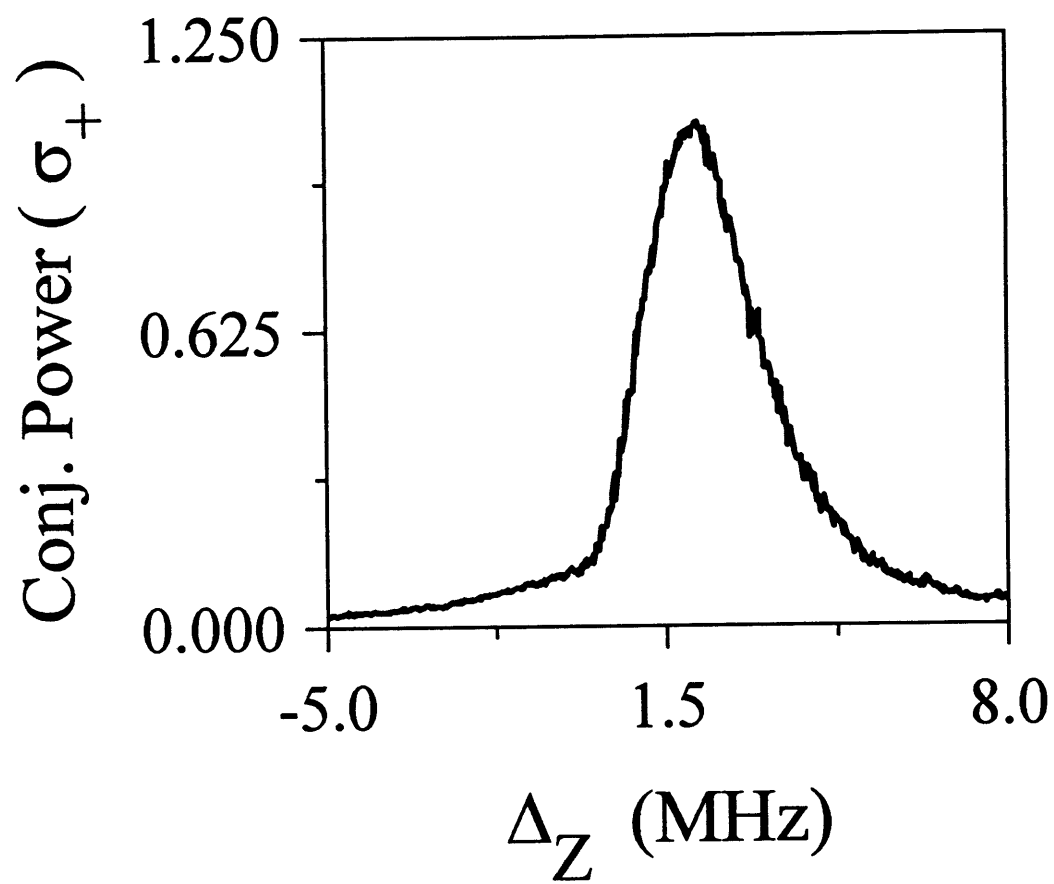


Figure 4.6: Sensitivity of the conjugation to the Zeeman shift.

an order of magnitude of the real result by renormalizing the power of the conjugate with the saturation measured (ie, conjugate power as a function of probe power). The result is in fact a kind of average of the linewidth over the range of probe power. Figure 4.7 shows the conjugate power versus the probe power and the fit that has been done for normalization.

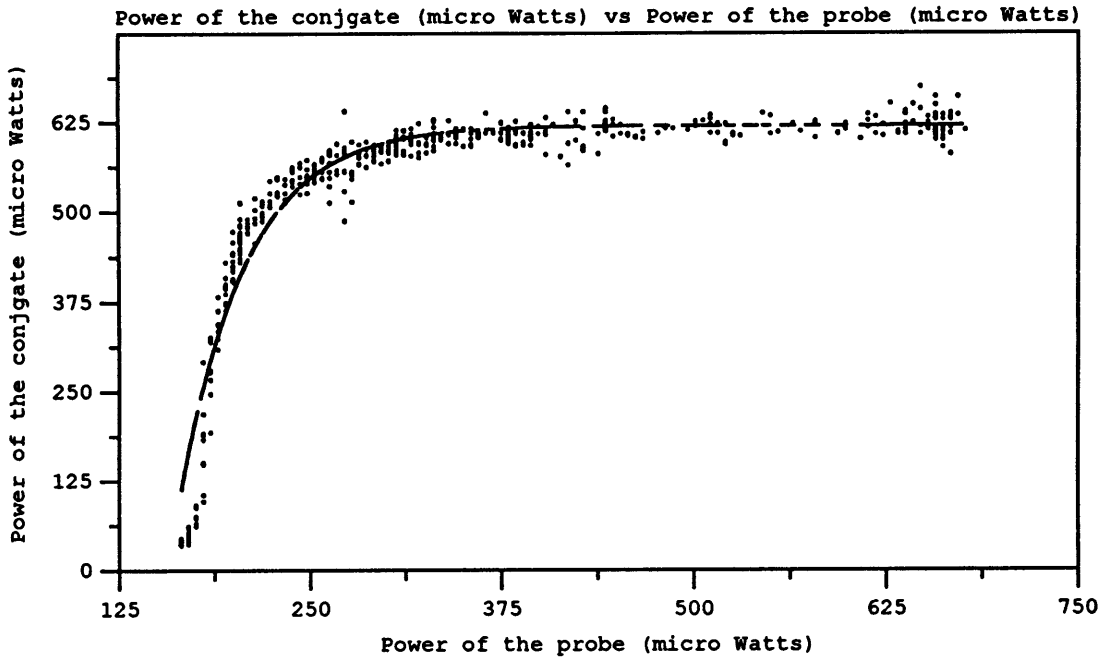


Figure 4.7: Saturation of the conjugation.

Figure 4.8 shows the renormalized conjugate power, this method gives a FWHM linewidth of 3.4 MHz, which is consistent with the previous result. We can still reasonably expect the real result to be closer to 2.4 MHz.

Assuming a linewidth of 2.4 MHz, we can obtain the response time of the process¹, for the given experimental conditions:

$$\tau_R = \frac{1}{2\pi\Delta\nu} = 6.6 \cdot 10^{-8} \text{ s}$$

The response time is 66 ns, which is good. Since we are already using low

¹ Assuming that the linewidth is primarily due to the optical pumping rate g^2/Γ

power, this keeps open the possibility of using semi-conductor lasers.

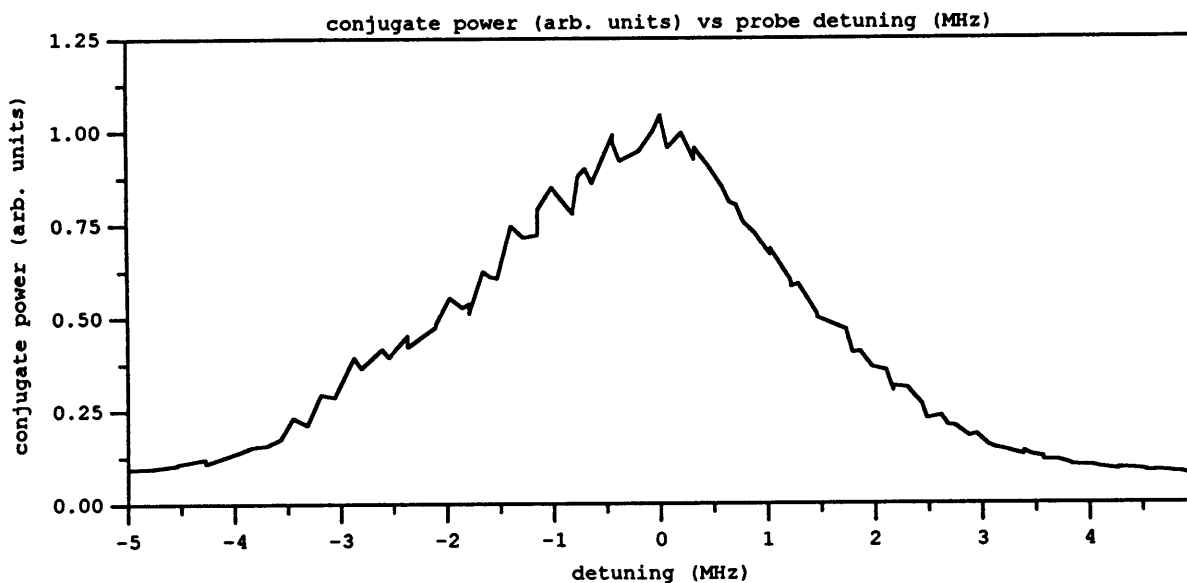


Figure 4.8: Renormalized lineshape.

4.2 Additional Results:

Broadening of the Linewidth:

Figure 4.9 shows a study of power broadening of the linewidth of the OPC effect. It has been done using Zeeman shifting, with three different power settings. These results show a slightly broader linewidth than before, but corresponds to conditions where a better efficiency has been obtained (cf Reflectivity study later). The power used and the linewidth are for each case:

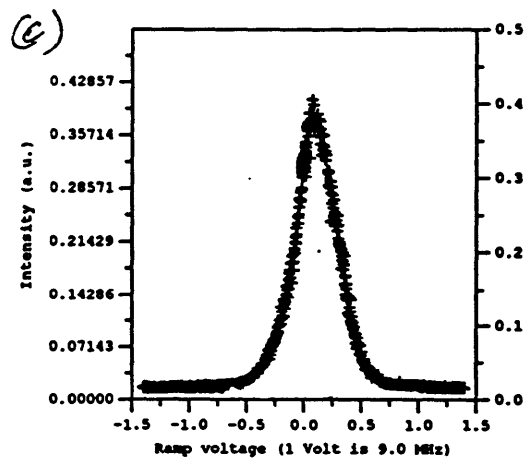
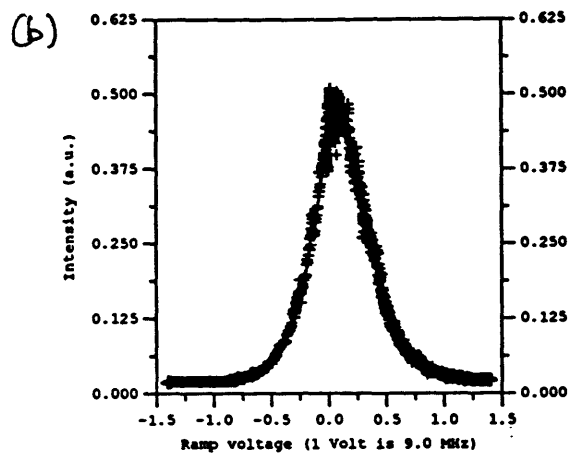
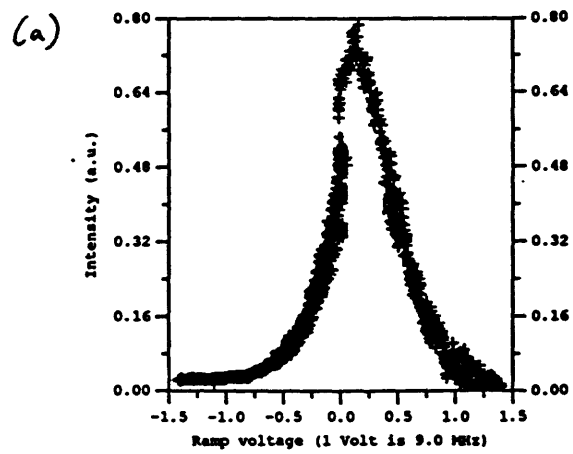


Figure 4.9: Lineshapes for different powers.

Case	$F(mW)$	$B(mW)$	$P(mW)$	$FWHMwidth(MHz)$
(a)	15.8	19.6	0.8	6.0
(b)	7.8	9.9	0.42	4.6
(c)	5.0	6.3	0.5	3.8

Sensitivity to One Pump Polarization:

To check that proper polarization was essential, we rotated the halfwave plate on the backward side, so that the polarization of the backward beam was rotated by twice that angle before going through the quarterwave plate. This means that if the plate is rotated by 45° , then the polarization is rotated by 90° . Crossing the quarterwave plate then forms a σ_+ polarization (like the forward beam). It is then expected that the conjugate disappears.

Figure 4.10 shows the experimental result, and indeed we see that a 45° rotation kills the conjugation. Furthermore a 2 to 1 elliptical polarization is already twice as less efficient as a perfect circular polarization.

Reflectivity:

Figure 4.11 (a) shows a result that was obtained with the same conditions as the broadening study (strongest power). Under these conditions, we can see that we get a peak reflectivity of about 10, at the onset of saturation, as can be seen on figure 4.11 (b).

Other Lines:

Those results, shown on figure 4.12, were obtained before the final polarization setup was made. Thus, it cannot be compared with the final results, but still can show the possibility of getting conjugation for different lines of the D1 manifold. In particular note that the conjugate for the $F = 1 \rightarrow F' = 1$ transition (for ^{87}Rb) is quite strong. This is the simplest of all possible cases, and will be the easiest when comparing to complete calculations to be performed in the near future.

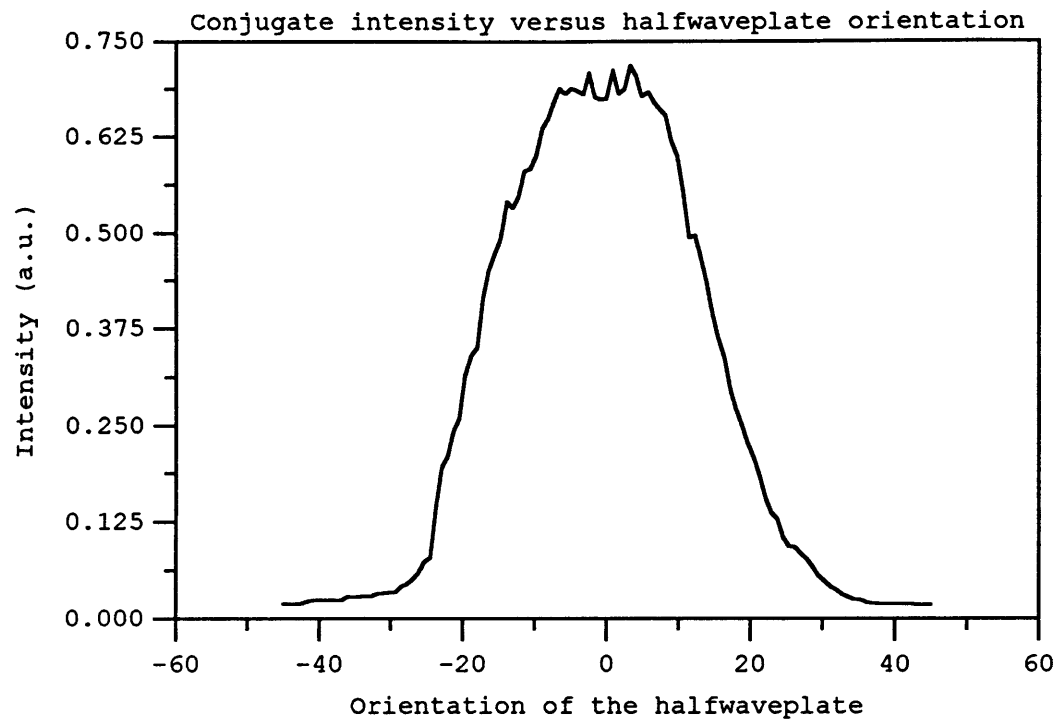
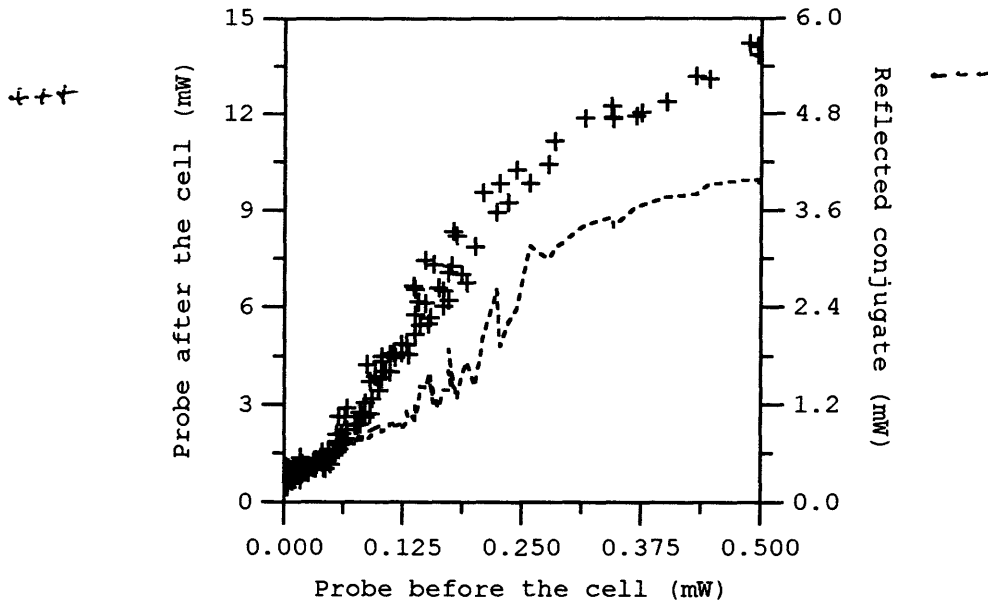


Figure 4.10: Sensitivity of the conjugate to the backward beam polarization.

(a)



(b)

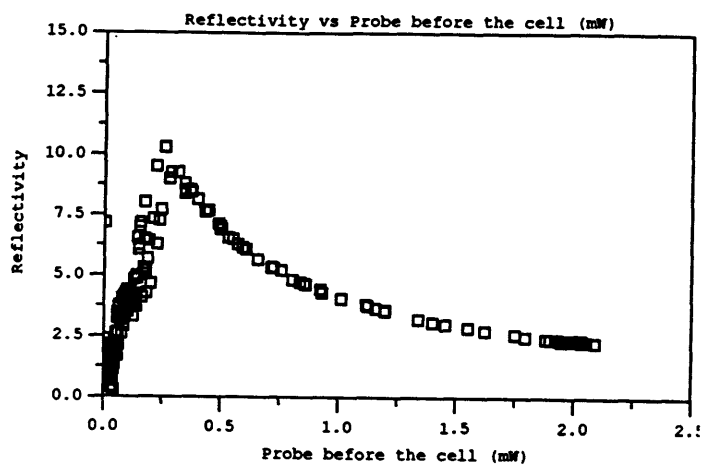


Figure 4.11: (a) Raw result (b) Reflectivity.

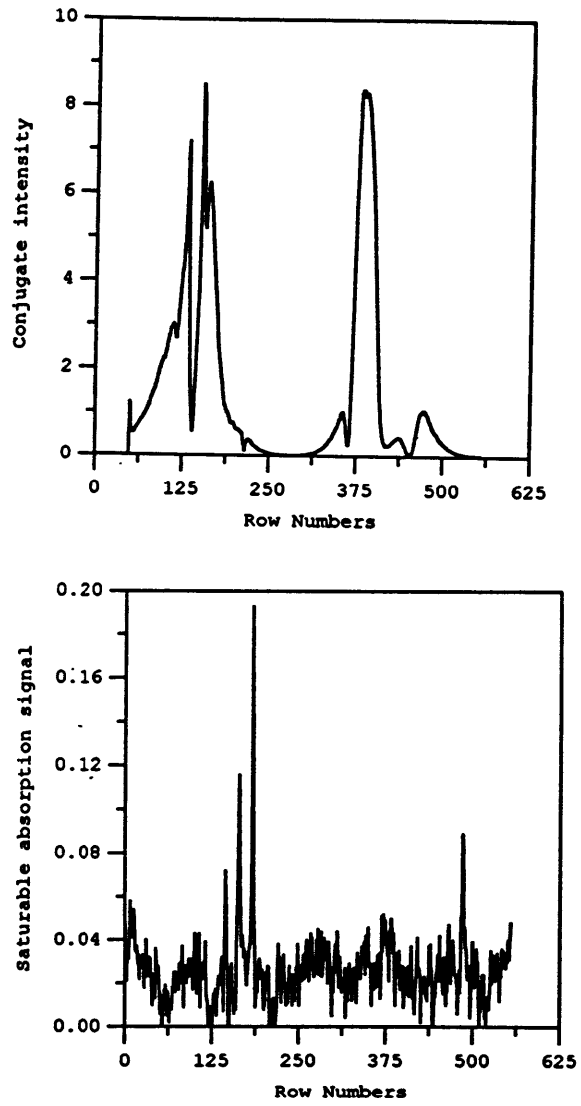


Figure 4.12: (a) Conjugation on the upper frequencies D1 lines (b) Corresponding saturable absorption signal.

Chapter 5

Summary And Conclusions:

5.1 Summary and Conclusions:

Optical phase conjugation (OPC) with low power and fast response is of interest in many applications. Generation of squeezed light, phase conjugation mirror, optical correlation and turbulence correction are the most promising examples.

Dye lasers and sodium atomic vapor have been used earlier within this group to demonstrate conjugation via hyperfine coherence gratings induced by coherent population trapping (CPT) in a Λ system. This resulted in a fast OPC (response time of about $1 \mu\text{s}$) with low pump intensities (about 1 W/cm^2). However this technique required that the probe be generated from the pump by coherent modulation at the hyperfine frequency difference of 1.77 GHz . In order to extend this technique to arbitrary atomic systems, one would require techniques for modulations at very high frequencies ranging from a few GHz (eg 6.8 GHz for rubidium, 9.2 GHz for cesium) up to hundreds of GHz (eg calcium and magnesium). As such, this technique is severely limited in practicality.

In order to circumvent this problem, we demonstrate in this thesis a new technique which uses the Zeeman sublevels within a hyperfine level as the two low-lying states of a Λ -transition. Specifically, we used the $5^2S_{1/2}, F = 2 \rightarrow 5^2P_{1/2}, F = 1$ transition of ^{87}Rb to demonstrate a reflectivity of 10 with a response time of 50 ns , using pump intensities of 2 W/cm^2 . Although we used a titanium:sapphire laser, these intensities are easily achievable using semi-conductor lasers, thus making it a very practical OPC system.

The mechanism in this process uses the polarization dependence of the Zeeman sublevels transitions to provide orthogonality between the two legs of the Λ transition. CPT caused by interaction of the forward pump and probe beam creates a coherence grating between the $m=-1$ and $m=+1$ Zeeman sublevels. The backward pump scatters off of this grating to produce the conjugate beam.

The simple level structure of the transitions involved enables us to demonstrate clearly the essential features of CPT in this process. For example, we find that the conjugate has the expected sensitivity to the polarization of the backward pump. We also observed a two-photon transition linewidth of 2.3 MHz , substantially below the single photon linewidth of 5.8 MHz .

As an additional result, we note that OPC was obtained for other lines of the D1 transition set. Broadening of the two-photon transition linewidth was also observed when the power of the beams are raised, making possible even shorter response times if required. Finally, we verified that the probe was amplified by the OPC process.

5.2 Future work:

The logical next step would be to try to modify the current rubidium setup towards a more ‘real life’ system. The two pumps should be replaced by two stabilized semi-conductor lasers¹, and a more compact cell could be built since some good experimental conditions have already been found.

The response time of the system can be studied by another approach, like using high speed RF switches to control the AOMs output. This would give another experimental proof of the speed of the OPC effect.

Application of this scheme could be made to other systems, like cesium (850 nm) or lithium (670 nm) in a similar way, but could also be made with calcium or magnesium where the double-lambda system is simply impossible due to the large separation of the ground states (hundreds of GHz).

Finally, we can mention promising applications like turbulence aberration correction, spatially broadband squeezing and ultrafast image correlation.

¹The only condition for writing the grating is indeed correlation between the forward and probe beams.

References:

1. For a review of OPC see, for example, R. A. Fisher, *Optical Phase Conjugation* (Academic, New York, 1983)
2. M. S. Shahriar and P. R. Hemmer in *Annual Meeting*, Vol. 6, 1995, *OSA Technical Digest Series* (Optical Society of America, Washington, D.C., 1995), p. 182
3. I. Biaggio, J. P. Partane, B. Ai, R. J. Knize and R. W. Hellwarth, *Nature* (London) Vol. 371, p. 318 (1994)
4. P. R. Hemmer, D. P. Katz, J. Donoghue, M. S. Shahriar and P. Kumar, *Opt. Lett.* Vol. 14, p. 245 (1991)